UNCLASSIFIED
SECURITY CLASSIFICATION OF THIS PAGE

REPORT DOCUMENTATION PAGE

Form Approved
OMB No. 0704-0188

1a. REPORT SECURITY CLASSIFICATION UNCLASSIFIED	1b. RESTRICTIVE MARKINGS
2a. SECURITY CLASSIFICATION AUTHORITY	3. DISTRIBUTION / AVAILABILITY OF REPORT
2b. DECLASSIFICATION / DOWNGRADING SCHEDULE	Approved for public release; distribution unlimited.

4. PERFORMING ORGANIZATION REPORT NUMBER(S)	5. MONITORING ORGANIZATION REPORT NUMBER(S)
G. L. Report No. 4680	

6a. NAME OF PERFORMING ORGANIZATION Stanford University	6b. OFFICE SYMBOL (If applicable)	7a. NAME OF MONITORING ORGANIZATION Office of Naval Research

6c. ADDRESS (City, State, and ZIP Code) Edward L. Ginzton Laboratory Stanford University Stanford, California 94305	7b. ADDRESS (City, State, and ZIP Code) Physics Division, Code 1112 Arlington, VA 22217-5000

8a. NAME OF FUNDING / SPONSORING ORGANIZATION	8b. OFFICE SYMBOL (If applicable)	9. PROCUREMENT INSTRUMENT IDENTIFICATION NUMBER N00014-87-K-0447

8c. ADDRESS (City, State, and ZIP Code)	10. SOURCE OF FUNDING NUMBERS

PROGRAM ELEMENT NO.	PROJECT NO.	TASK NO.	WORK UNIT ACCESSION NO.
61153N	4126945		

11. TITLE (Include Security Classification)

Millimeter-Wave Acoustic Transducers   UNCLASSIFIED $ADA\ 221402$

12. PERSONAL AUTHOR(S)
by C. F. Quate, L.J. LaComb, Jr., and D.R. Wright

13a. TYPE OF REPORT Final Report	13b. TIME COVERED FROM 06/01/87 TO 09/30/89	14. DATE OF REPORT (Year, Month, Day) April 1990	15. PAGE COUNT 74

16. SUPPLEMENTARY NOTATION

17. COSATI CODES			18. SUBJECT TERMS (Continue on reverse if necessary and identify by block number)
FIELD	GROUP	SUB-GROUP	Acoustics, Transducers, Liquid Helium, Parametric
20	01		Amplification, Zinc-oxide

19. ABSTRACT (Continue on reverse if necessary and identify by block number)

This project was focused on a program to realize efficient systems for generating and detecting coherent phonons with millimeter wavelengths. The primary task was the realization of transducers that are capable of converting electromagnetic energy to acoustic energy in this frequency region. In order to increase the operating frequency, the components of the acoustic transducer must be redesigned. Instead of the single layer ZnO acoustic transducers used below 10 GHz, multilayer ZnO acoustic transducers must be used to generate sufficient power at frequencies above 24 GHz. In association with all of this we have continued to investigate the nature of acoustic wave propagation in liquid helium.

20. DISTRIBUTION / AVAILABILITY OF ABSTRACT ☒ UNCLASSIFIED/UNLIMITED ☐ SAME AS RPT ☐ DTIC USERS	21. ABSTRACT SECURITY CLASSIFICATION UNCLASSIFIED
22a. NAME OF RESPONSIBLE INDIVIDUAL L. E. Hargrove, ONR Physics Division	22b. TELEPHONE (Include Area Code) (202) 696-4221	22c. OFFICE SYMBOL ONR Code 1112

DD Form 1473, JUN 86   Previous editions are obsolete.   SECURITY CLASSIFICATION OF THIS PAGE

$ADA\ 221402$

Edward L. Ginzton Laboratory
W. W. Hansen Laboratories of Physics
Stanford University
Stanford, California 94305

Millimeter-Wave Acoustic Transducers

Final Report

for the period

June 1, 1987 - September 30, 1989

Office of Naval Research

Contract No. N00014-87-K-0447

Principal Investigator

C. F. Quate

G. L. Report No. 4680

April 1990

TABLE OF CONTENTS

Final Report

Millimeter-Wave Acoustic Transducers

June 1, 1987 - September 30, 1989

I. Introduction

This project was focused on a program to realize efficient systems for generating and detecting coherent phonons with millimeter wavelengths. The primary task was the realization of transducers that are capable of converting electromagnetic energy to acoustic energy in this frequency region.

In order to increase the operating frequency, the components of the acoustic transducer must be redesigned. Instead of the single layer ZnO acoustic transducers used below 10 GHz, multilayer ZnO acoustic transducers must be used to generate sufficient power at frequencies above 24 GHz. These multilayer ZnO transducers have been used to generate approximately 28 GHz sound with two-way conversion losses as low as 27 dB. Multilayer transducers have also been fabricated for operation at frequencies as high as 100 GHz, where the two-way conversion loss is approximately 50 dB. These ZnO multilayer transducers represent the highest operating frequency of any ZnO transducer and the highest conversion efficiencies for any type of transducer in this frequency range. The theoretical aspects of multilayer transducers were explored along with experimental verification of some theoretical predictions. The possibility of generating sound at frequencies as high as 300 GHz has been considered.

A piezoelectric mechanical scanning system was designed for operation at temperatures as low as 100 milliKelvin. The scanner is able to overcome the loss in sensitivity of the piezoelectric elements at low temperatures by using lever arms to magnify the piezoelectric motion. The resolution, frequency characteristics, and heat dissipation properties of the scanner are presented.

In association with all of this we have continued to investigate the nature of acoustic wave propagation in liquid helium. This liquid is suitable for propagating sound waves at these ultrahigh frequencies and our goal was to study the linear and nonlinear properties of this medium.

As a final effort near the end of this period we co-operated with research workers at the Aerospace Corporation in El Segundo to construct a scanning acoustic microscope operating at 15.3 GHz with a resolution of 150 Å.

II. Millimeter-wave Acoustic Transducers

Previous generations of water and cryogenic acoustic microscopes used thin film piezoelectric transducers to generate and detect the acoustic signal used for imaging. These transducers usually consist of a vacuum deposited thin film of piezoelectric material sandwiched between two metal electrodes. An rf-voltage is applied across the electrodes and acoustic waves are generated in the piezoelectric material. In a reciprocal manner, acoustic waves entering the piezoelectric material generate a voltage across the electrodes which can be sensed and recorded. Such transducers generally operate at thickness-mode resonance and are probably the most efficient generators and detectors of acoustic waves for frequencies ranging from a few hundred Megahertz up to 10 GHz.[1,2] Thin film transducers are capable of generating and detecting both shear and longitudinal waves depending on the orientation of the piezoelectric material with respect to the applied electric field. A large variety of materials have been used to generate microwave frequency acoustic waves including ZnO, CdS, and $LiNbO_3$. In transducers reported here, ZnO was chosen because of its high coupling coefficients and ease of vacuum deposition. At frequencies above 10 GHz, the performance of these simple acoustic transducers is impaired by two factors. The conversion efficiency typically becomes quite small for reasonably sized transducers and the failure rate from fabrication defects increases with the decreasing thickness of the transducer. In order to extend the operating frequency of the acoustic microscope, a new approach to the transducer construction was needed. This chapter describes the design, fabrication and evaluation of multilayer ZnO acoustic transducers in the frequency range of 25-100 GHz and explores the possibility of using multilayer ZnO transducers to generate sound at frequencies above 100 GHz.

1. Rational for Multilayer Transducers

The conversion loss of a thickness-mode resonant transducer can be separated into two parts:

2

$$CL(dB) = CL_{ac}(dB) + CL_{el}(dB) \qquad (2.1)$$

where CL_{ac} is the part due to the acoustic losses in the system and CL_{el} is the part due to the electrical losses in the system. Eq. (2.1) can be simplified for many microwave transducers. In most microwave applications, the thicknesses of the electrodes are small compared to an acoustic wavelength and their effect on the conversion loss can be neglected. If there are no acoustic matching layers in the system, the electrical losses dominate the acoustic losses since most thin-film materials have high acoustic Q's. The electrical loss can be characterized by:[1]

$$CL_{el}(dB) = 10 \log \left[\frac{4 R_s R_a}{\left(R_s + R_{se} + R_a \right)^2 + \left(X_{se} + X_a \right)^2} \right] \qquad (2.2)$$

where R_s is the source impedance, R_a is the real part of the transducer impedance, X_a is the imaginary part of the transducer impedance. R_{se} and X_{se} represent the real part and imaginary part of the stray series impedance that usually arises from the physical connection of the transducer to the source. For most applications, R_s is typically 50Ω, R_{se} and R_a are on the order of 1Ω, and X_{se} is usually small until very high frequencies. If $X_a \ll R_s$, Eq. (2.2) can be approximated by:

$$CL_{el}(dB) = 10 \log \left[\frac{4 R_a}{R_s} \right]. \qquad (2.3)$$

Because R_s is set by the equipment, the major factor affecting the conversion loss is R_a.

If the acoustic losses are small and the thickness of the metal electrodes is much less than the sound wavelength, the real part of the transducer impedance at resonance can be approximated as:

$$R_{a0} = \frac{4k_t^2}{\pi r_d \omega_0 C_0} \qquad (2.4)$$

where k_t is the piezoelectric coupling constant of the material, r_d is the ratio of the mechanical impedances of the thin film and the substrate, ω_0 is the angular frequency at the half-wave resonance and, C_0 is the clamped capacitance of the transducer. The clamped capacitance of the transducer is inversely proportional to the half-wave thickness and proportional to the resonant frequency. Thus, for a fixed r_d, the radiation resistance decreases as the resonant frequency squared. The result of Eqs. (2.3) and (2.4) is that if one simply tries to scale the center frequency of the transducer from 10 GHz to 100 GHz, the two-way untuned conversion loss increases by 40 dB as can be seen in Fig. 2.1.

Several methods have been proposed to increase the conversion efficiency at high gigahertz frequencies. The conversion loss can be improved at the expense of reduced bandwidth by electrically tuning the transducer to cancel the impedance mismatch between the source and transducer. If the impedance mismatch were able to be perfectly compensated, a difficult task at millimeter-wave frequencies, the tuned conversion loss would be:

$$CL_{el}(dB) = 10\log\left[\frac{R_a}{R_s + R_{se}}\right]. \qquad (2.5)$$

At millimeter-wave frequencies, two factors dominate the series resistance. Most methods for attaching the transducer to the rf source employ thermo-compression bonding to the top electrode which generates some resistance at the bond interface. The other major factor affecting the series resistance is the small skin depth of the rf signal at high frequencies which leads to high surface resistivities. These two factors usually place a lower limit on the series resistance of about 1 Ω. The impedance of a single layer transducer can be estimated from Eq. (2.4). A 60 μm radius ZnO transducer operating at a center frequency of 100 GHz on a sapphire substrate would have an impedance of less than 0.01Ω. Even in such a best case example, the tuned one-way conversion
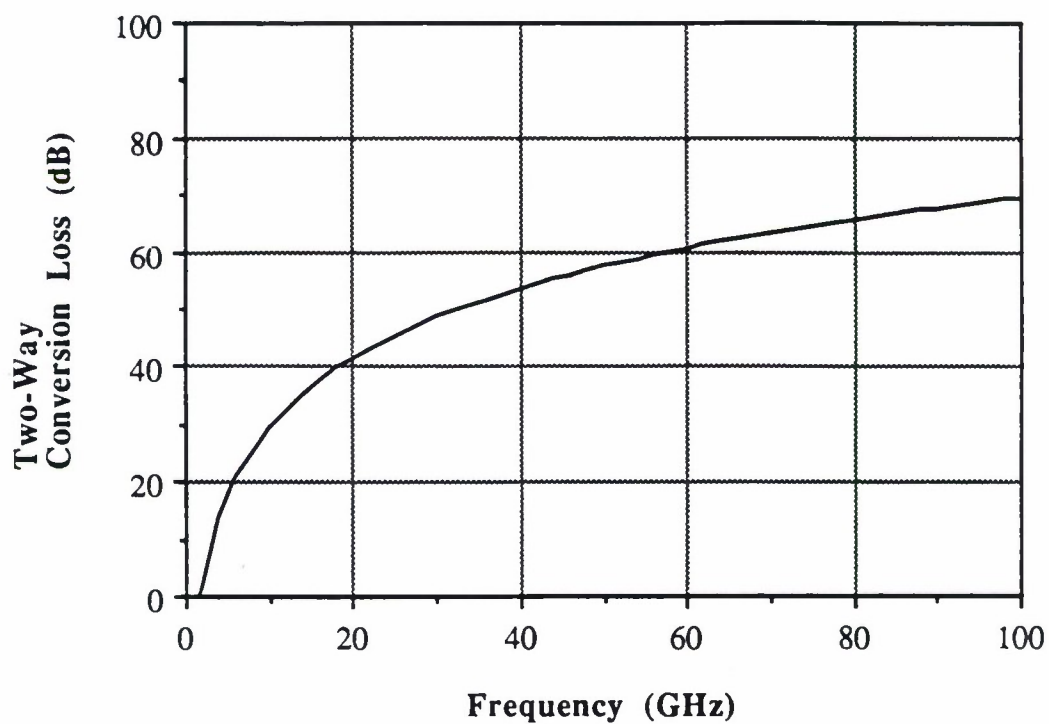
Figure 2.1 Two-way conversion loss of a thin-film transducer as a function of frequency. Transducers radius = 60 μm, sapphire substrate.

loss would still be approximately 20 dB making tuning alone an impractical approach to the problem.

Another possible solution is to increase the transducer's impedance by decreasing the transducer radius. In the high frequency water microscope, transducers with radii as small as 30 μm have been used.[3] In the helium acoustic microscope, reducing the transducer radius would require decreasing the lens radius to maintain uniform aperture illumination.[3,4] In addition to the difficulties in the precise machining of a smaller lens opening, the overall length of the lens would have to be reduced to ensure proper illumination.[3] To overcome the small reduced path length in the sapphire, shorter pulses would have to be used at larger bandwidths-leading to higher noise levels and reduced dynamic range. Because of the numerous detrimental side effects, reducing the transducer's radius as the sole method of improving the conversion efficiency is undesirable.

The second problem encountered in using single layer acoustic transducers at millimeter wave frequencies is that the small thickness of the transducer would often lead to shorting between the two metal electrodes rendering the transducer inoperative. Such shorting was observed in transducers fabricated for operation at 8 GHz where the ZnO is approximately 2000 Å thick.[3] Near 100 GHz, the typical thickness for a ZnO transducer would be a few hundred Ångstroms increasing the likelihood of pinholes. The occurrence of pin-hole defects can be reduced by improving the sputtering uniformity; however, at millimeter wave frequencies shorting between the electrodes could still be a serious problem.

2. Multilayer Theory

In an effort to overcome the high conversion loss associated with high frequency thin film transducers, Shaw[5] and de Klerk[6] proposed that multilayer transducers be used. In a multilayer transducer, piezoelectrically active layers alternate with passive or piezoelectrically less active layers to form an acoustic resonator. For maximum conversion efficiency, the thickness of each layer should be one-half an acoustic wavelength for that material. Early work concentrated on CdS as the active material and SiO[6] as the passive material. In the early 1970's, the advent of superlattices made it theoretically possible for coherent phonon generation with frequencies into the

6

infrared.[7,8] Other authors[9,10] have suggested that a nonpiezoelectric semiconductor with periodic doping in the pattern *n* doped-*i*ntrinsic-*p* doped-*i*ntrinsic-*n-i-p-i*... could be used to generate high frequency coherent phonons via Coulomb forces between the accumulated charges at the interfaces.

Recently, Hadimioglu *et al*[11] reported a new fabrication technique for multilayer transducers. This technique exploits the fact that ZnO, and all hexagonal crystals, exhibit a maximum in the longitudinal wave coupling when the c-axis is oriented parallel to the applied electric field and a minimum at approximately 40 degrees from the electric field.[12] Other researchers[13] have shown that "tilted" ZnO can be grown at an oblique angle to the c-axis by tilting the substrate and positioning it near the edge of the plasma in the deposition station. By altering the c-axis, and thus the longitudinal wave coupling, a multilayer transducer can be assembled one layer at a time as shown in Fig. 2.2. The ZnO is deposited by dc-magnetron sputtering using a zinc target in a 80%-20% oxygen-argon atmosphere. The basic ZnO deposition system used in depositing single layer ZnO transducers has been modified so that the substrate can be positioned at three different locations as shown in Fig. 2.3(a). In position I, the substrates are parallel to the ZnO target and centered over the target. When deposited in this configuration, the ZnO grows in the "normal" orientation yielding a high longitudinal piezoelectric coupling coefficient. In position II, the substrates are rotated 40° with respect to the ZnO target normal. The center of the substrate holder is also moved a distance **d** = 1.5 inches from the location at position I. ZnO deposited in this "tilted" position yields a smaller longitudinal piezoelectric coupling constant. ZnO deposited in position III has similar characteristics to that deposited at position II. Both positions are used to ensure that any thickness variations in the direction parallel to the substrate holder are minimized. The substrate holder is moved between the positions in the pattern I-II-I-III-I-II... until the desired number layers have been deposited. As can be seen in Fig. 2.3(b), the substrate holder does not have circular symmetry. This anisotropy can lead to transducers with different performance characteristics and center frequencies depending on the substrate location.
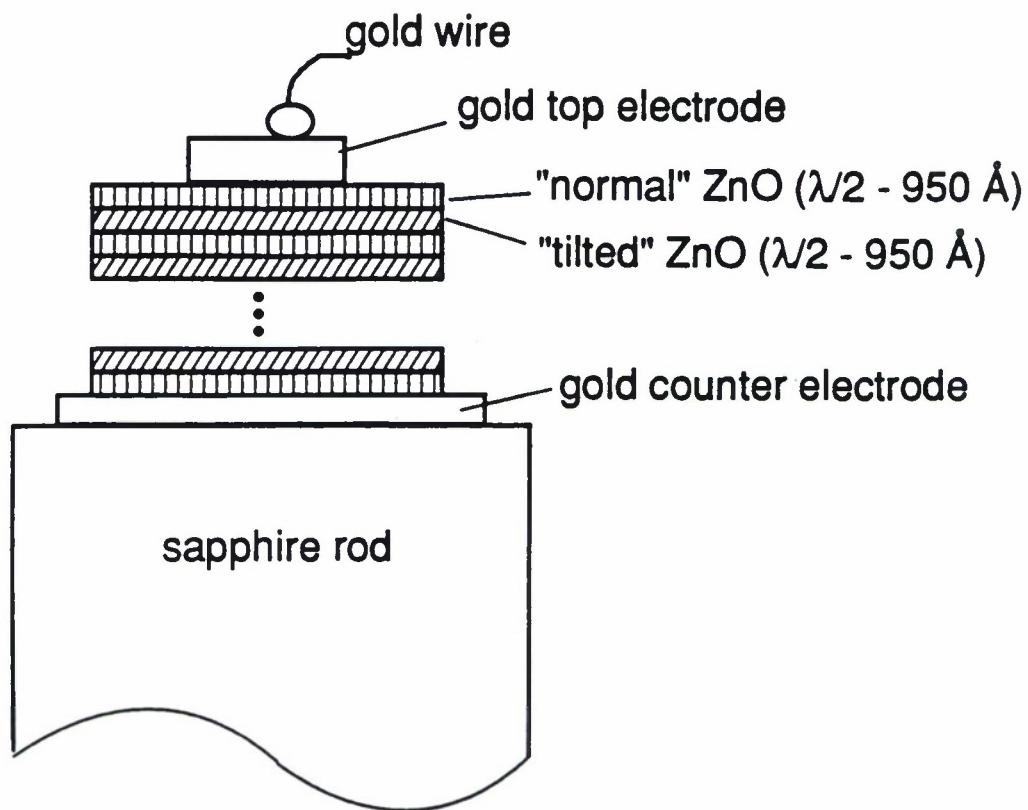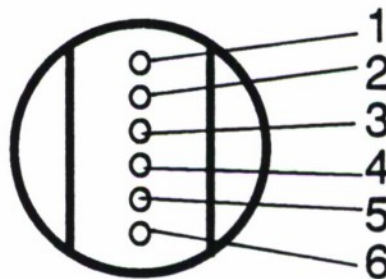
Ka-BAND TRANSDUCER GEOMETRY

Figure 2.2 Ka-Band transducer geometry.
Schematic showing the basic elements of a multilayer transducer.

Zn target
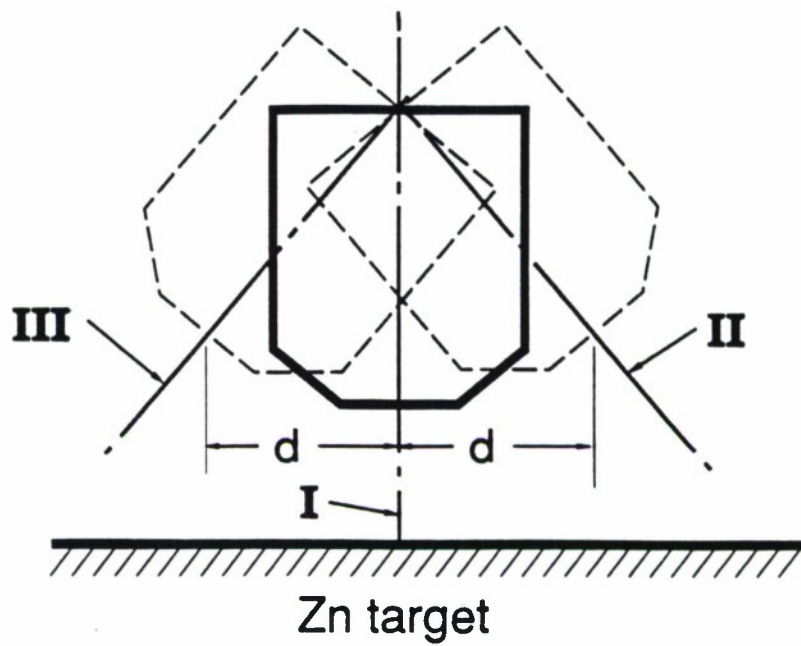
(a)

holes for substrates

(b)

Figure 2.3 Multilayer transducer deposition schematic.
(a) In position I the ZnO is deposited in the "normal" normal orientation, in positions II and III the ZnO is deposited in the "tilted" orientation. (b) The "head on" view of the sample holder showing the lack of circular symmetry.

The method described above offers several advantages over other methods proposed to date. Because only ZnO is used in the transducer fabrication, the entire deposition can be done in a single pump-down in a dedicated vacuum station, whereas the CdS multilayer transducers used other components for the passive layers. Because the transducers can be deposited in a single pump-down of the vacuum system, the chances of contamination are minimized and the repeatability of the results is enhanced. Two component multilayer transducers also present additional problems regarding lattice mismatch between the layers[8] and stresses developed by differences in the thermal contraction of the layers between room temperature and typical cryogenic acoustic microscopic applications.

In order to get a feel for the advantages of a multilayer transducer, one can imagine building an ideal multilayer transducer. This transducer would be composed of N layers of an active piezoelectric material (A_i; i = 1...N) and N layers of a passive material (P_i ; i = 1...N) with the same acoustic impedance and electrodes so thin that their effect is negligible. Each of the layers would be one-half an acoustic wavelength thick and the acoustic attenuation would be zero. Such a transducer is shown in Fig. 2.4(a). Because the electromagnetic radiation pattern is of nearly constant phase between the electrodes, each of the active layers will have the same response as shown in Fig. 2.4(b). The acoustic wave entering the second active layer will have the same phase as the acoustic wave generated in that layer and the amplitudes will add as scalars. This process continues down the length of the transducer where the final amplitude will be N times the amplitude generated by a single period, Fig. 2.4(c). Therefore, the acoustic power delivered to the substrate is:

$$P_{ac} \propto A_{ac}^2 \propto N^2 \qquad\qquad (2.6)$$

where P_{ac} is the acoustic power, and A_{ac} is the acoustic wave amplitude. This simple analysis show the major advantage of the multilayer transducer, namely that the conversion efficiency of the transducer is proportional to the number of layers squared.
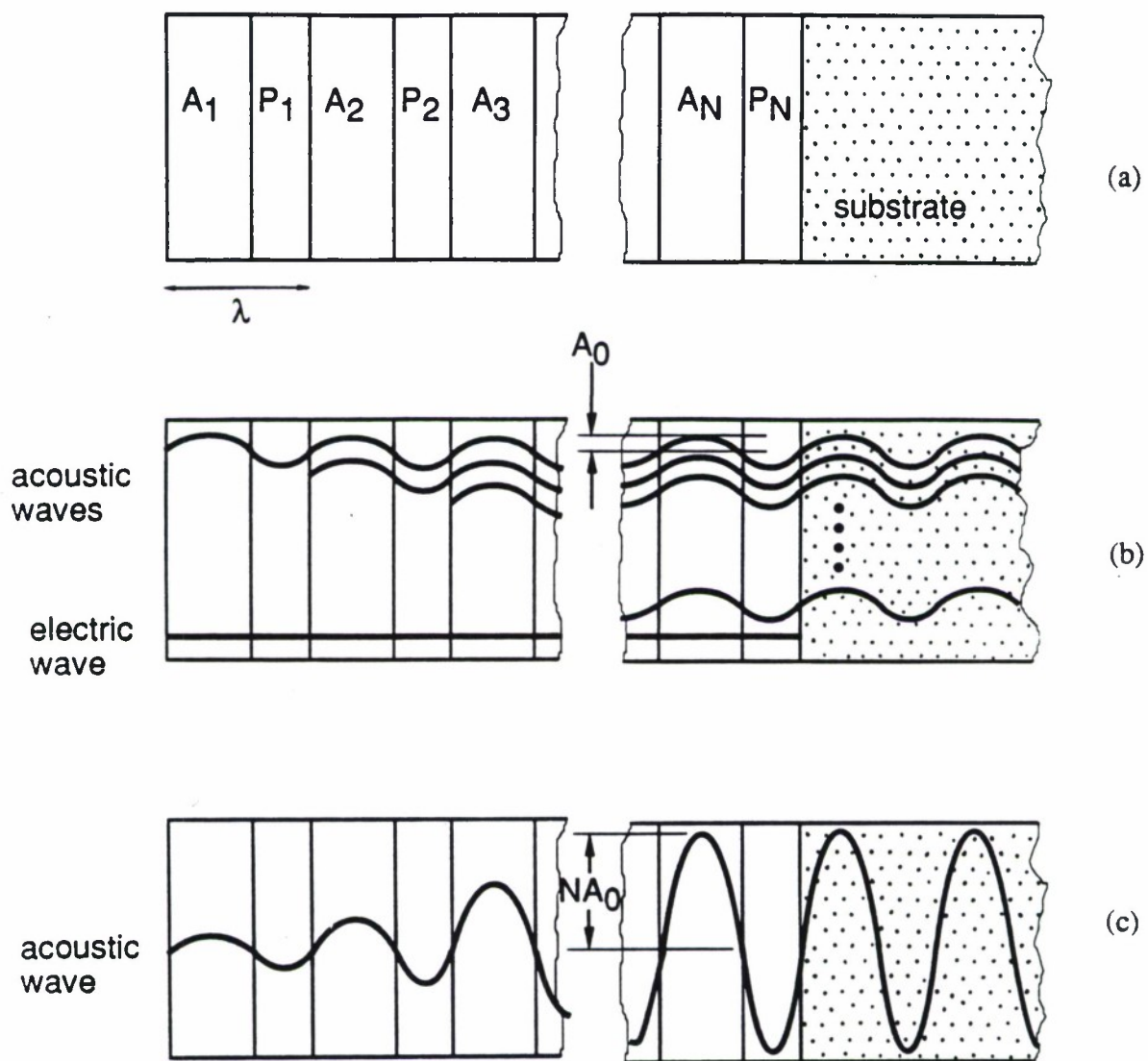
10

Figure 2.4 Acoustic wave amplification in a multilayer transducer.
(a) A transducer containing N active layers (A_i) and N passive layers (P_i). (b) Propagation of acoustic wave of amplitude A_0 generated at each interface. (c) Amplification resulting from all acoustic waves adding in phase.

11

A more complete analysis of the acoustic power generated by the multilayer transducer can be found in the analysis of Yang *et al* .[7] This analysis yields:

$$A_{ac}(Nt) = M(F_1 + F_2)$$ (2.7)

where:

$$M = \frac{1 - e^{j(k-q)Nt}}{1 - e^{j(k-q)t}}$$

$$F_1 = \int_{\varepsilon}^{t_1 - \varepsilon} f(z)\, dz + \int_{t_1 + \varepsilon}^{t_1 + t_2 - \varepsilon} f(z)\, dz \ \Big|_{\lim \varepsilon \to 0}$$

$$F_2 = \int_{t_1 - \varepsilon}^{t_1 + \varepsilon} f(z)\, dz + \int_{t_1 + t_2 - \varepsilon}^{t_1 + t_2 + \varepsilon} f(z)\, dz \ \Big|_{\lim \varepsilon \to 0}$$

$$f(z) = \frac{\partial(eE)}{\partial z} e^{-jqz} \left[2T\left(j\, qU(z) + \frac{\partial U}{\partial z}\right)\right]^{-1}$$ (2.8)

and $A_{ac}(Nt)$ is the amplitude of the acoustic wave entering the substrate, $U(z)$ is the displacement velocity which has the Bloch form $U(z) = U(z+nt)$, $E(z)$ is the electric field which also is of the Bloch form, e is the piezoelectric stress constant, q is the photon wavevector, k is the phonon wave vector, t_1 and t_2 are the thickness of the respective layers, and $t = t_1 + t_2$. The M coefficient in Eq. (2.7) is a maximum when $k \equiv q$ and takes on the value N. The F_1 term represents the contribution from the bulk and is usually negligible because for $\lambda_{el} \gg t$, $E(z) \approx$ const, and e(z) is constant within each layer. The main contribution comes from F_2 which represents the

contribution from the discontinuities at the boundaries. If the change in permittivity between the layers is small, $E(z)$ is approximately constant, and the differential term in $f(z)$ can be approximated by Δe. A more complete expression for Eq. (2.6) is:

$$P_{ac} \propto A_{ac}^2 \propto \left(N\Delta e\right)^2 \qquad (2.9)$$

indicating that both the number of layers and the difference in the piezoelectric constant between the layers affect the output power.

The reason for the high conversion efficiencies in a multilayer transducer can be seen by looking at the electromagnetic and acoustic dispersion curves for a multilayered media. When $q \equiv k$, the acoustic and electromagnetic wave are phase matched, this phase matching occurs whenever, in the reduced zone scheme, the photon dispersion curve intersects the phonon dispersion curve. At these points, the direct conversion of photons to phonons is permitted. The acoustic dispersion relation of a multilayered media in the continuum limit is given by:[14]

$$\cos(qt) = \cos\left(\frac{\omega t_1}{v_1}\right)\cos\left(\frac{\omega t_2}{v_2}\right) - \frac{1 + p_{ac}^2}{2p_{ac}}\sin\left(\frac{\omega t_1}{v_1}\right)\sin\left(\frac{\omega t_2}{v_2}\right) \qquad (2.10)$$

where $p_{ac} = v_1\rho_1/v_2\rho_2$, v_1 and v_2 are the sound velocities and ρ_1 and ρ_2 are the densities of their respective layers. In the continuum limit, the electromagnetic dispersion relation of a multilayered media is given by:[14]

$$\cos(kt) = \cos\left(\frac{\omega t_1}{c_1}\right)\cos\left(\frac{\omega t_2}{c_2}\right) - \frac{1 + p_{el}^2}{2p_{el}}\sin\left(\frac{\omega t_1}{c_1}\right)\sin\left(\frac{\omega t_2}{c_2}\right) \qquad (2.11)$$

where $p_{el} = \varepsilon_1\mu_2/\varepsilon_2\mu_1$, ε_1 and ε_2 are the permittivities, μ_1 and μ_2 are the permeabilities and c_1 and c_2 are the propagation velocities of electromagnetic radiation in the respective medium.

13

Since the layer thicknesses in a millimeter-wave ZnO multilayer transducer are on the order of a thousand Ångstroms or less, $\sin\left(\frac{\omega t}{c} \cong 0\right) \cong 0$ and $\cos\left(\frac{\omega t}{c} \cong 0\right) \cong 1$, the electromagnetic dispersion is a near vertical line with $k \approx 0$ for all frequencies in the millimeter-wave region. If the layers have similar acoustic properties, $p_{ac} \approx 1$, the acoustic dispersion relation becomes:

$$\cos(qt) = \cos\left(\frac{\omega t_1}{v_1} + \frac{\omega t_2}{v_2}\right) \tag{2.12}$$

Figure 2.5 is a plot of the electromagnetic and acoustic dispersion curves for an ideal multilayer transducer with a center frequency of 32 GHz. Because of the zone folding introduced by the periodicity of the multilayer transducer, it should also be possible to generate acoustics at all the harmonics of the fundamental frequency through *umklapp* processes. Because the F_2 term in Eq. (2.7) is the major source of the acoustic waves, gain occurs only at the odd harmonics of the fundamental as can be seen in Fig. 2.6. Fig. 2.6(a) is the fundamental resonance, the waves generated at each boundary are in phase and constructively interfere to produce the amplified acoustic wave. The second harmonic, Fig. 2.6(b), suffers destructive interference at each boundary and the resulting wave is negligibly small. The third harmonic, Fig. 2.6(c), is once again in phase with the wave generated in the next interface and the constructive interference produces an amplified acoustic wave.

In a non-ideal transducer, the values for p_{ac} and p_{el} will not be exactly unity, resulting in imaginary wave vectors in certain regions of frequency space, Fig. 2.7. These frequencies will suffer high attenuation rates and the conversion efficiency in these regions will be quite small. Fig. 2.7 also indicates that even in a non-ideal multilayer transducer there is still direct photon-to-phonon conversion at the intersection of the dispersion curves but, that in the non-ideal multilayer transducer there will also be frequencies where the conversion efficiency will be negligibly small. Non-ideal multilayer transducers should still have the same higher harmonic performance as the ideal transducer.
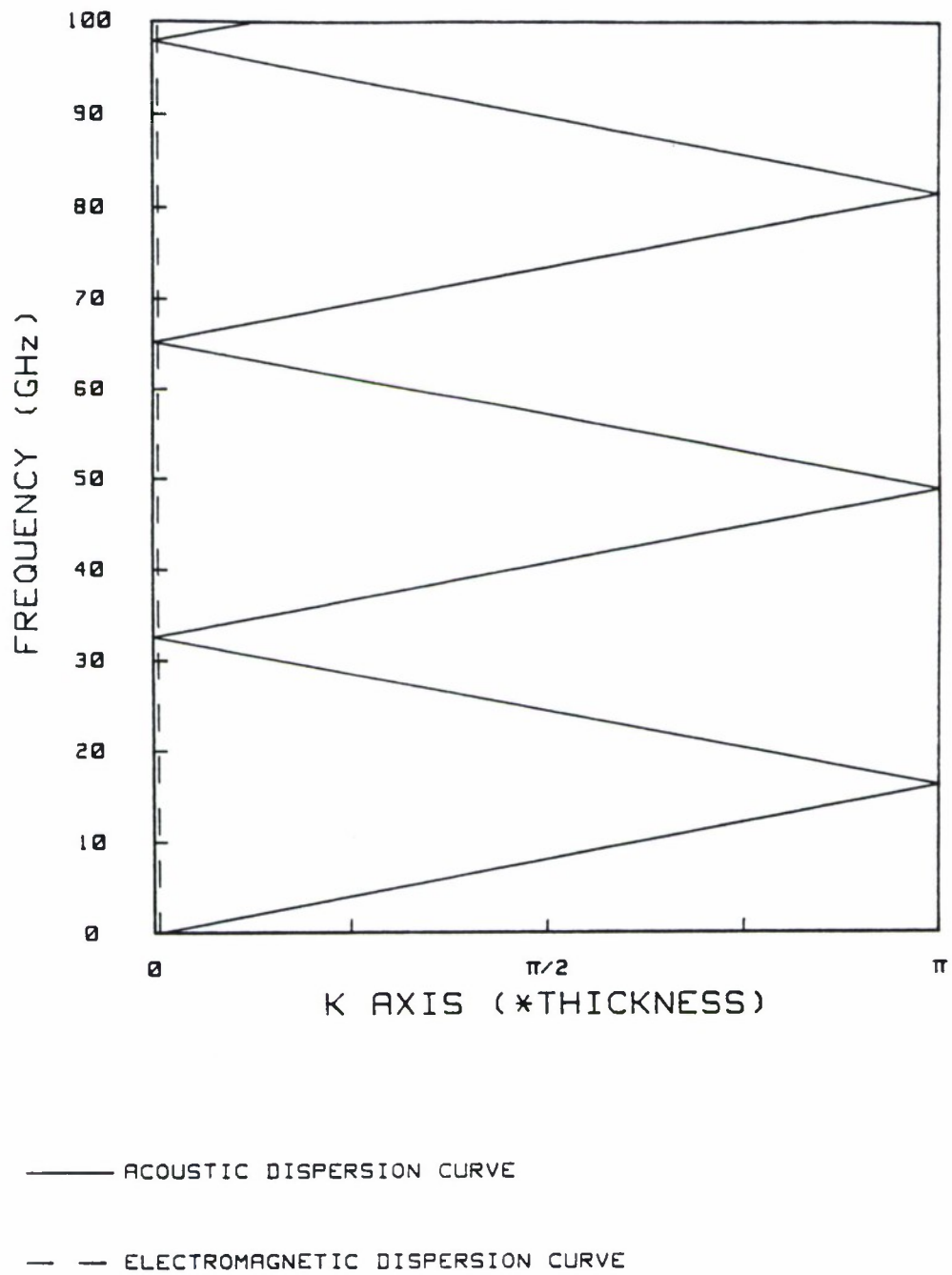
Figure 2.5 Acoustic and electromagnetic dispersion curves for an ideal multilayer transducer.
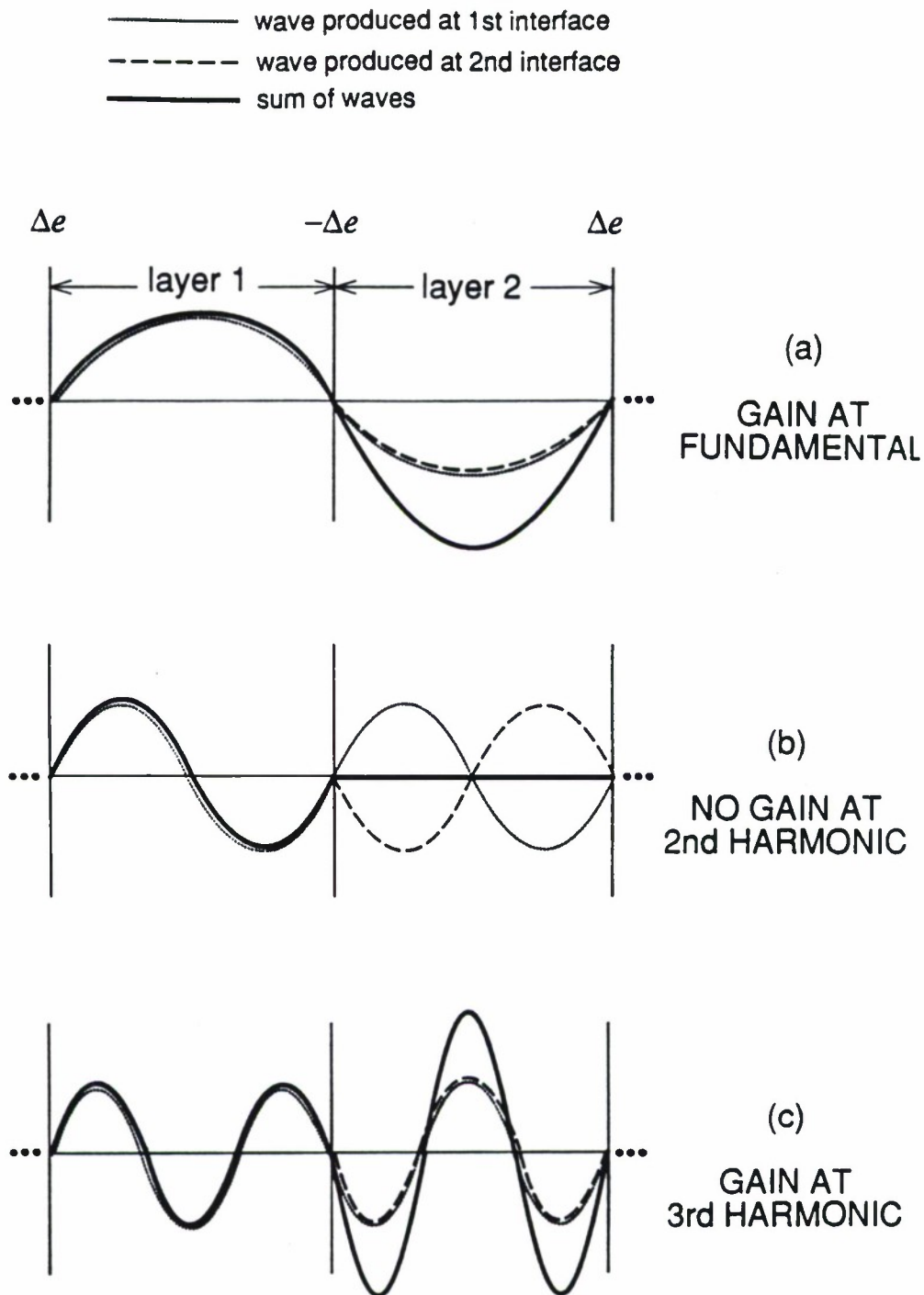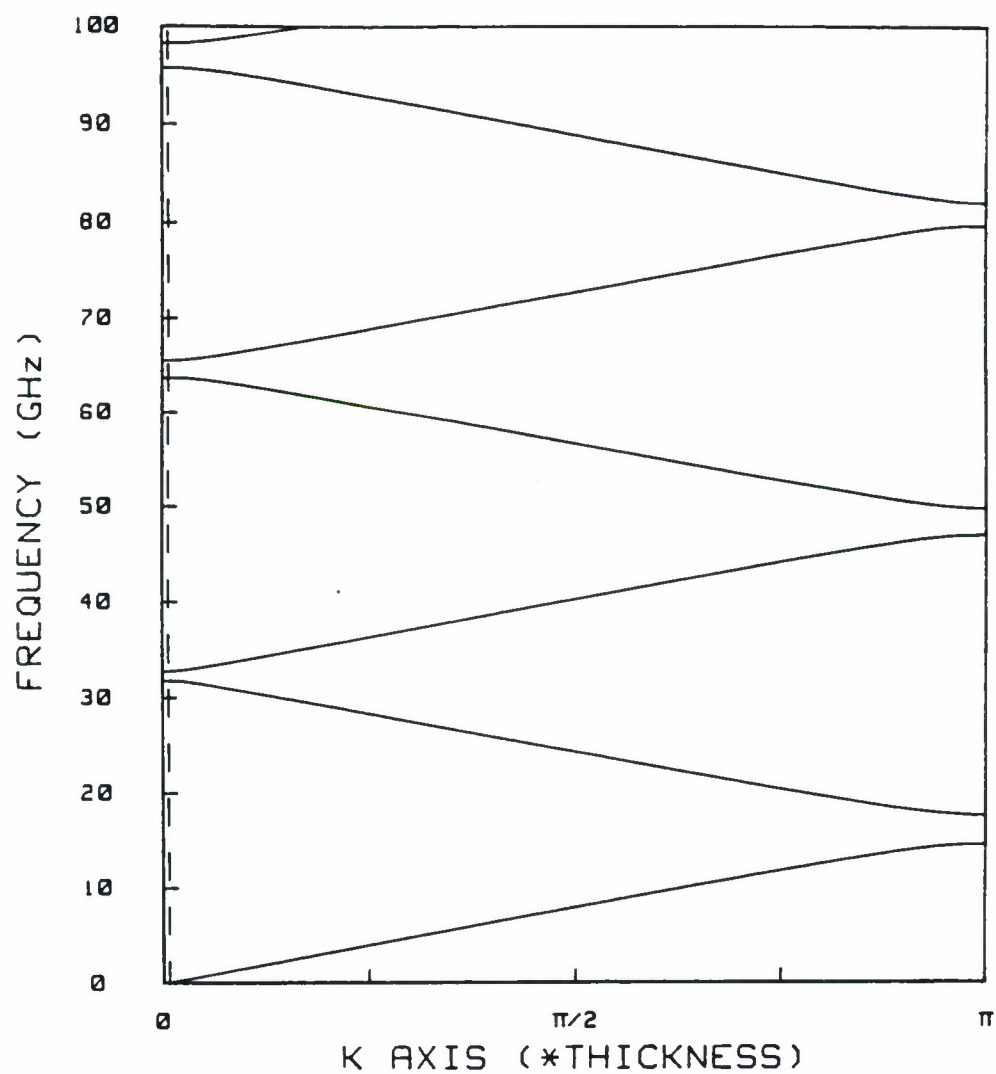
Figure 2.6 Interference effects at higher harmonics in a multilayer transducer.
(a) Amplification at fundamental due to constructive interference. (b) No amplification at
the second harmonic due to destructive interference. (c) Amplification at third harmonic
due to constructive interference.

Figure 2.7 Acoustic and electromagnetic dispersion curves for a non-ideal multilayer transducer.

3. Results

The theoretical models of the multilayer transducer usually contain an identical number of piezoelectrically active and inactive layers. In practice, an odd number of layers is used and an active layer is used for both the first and last layers. The reason for using an active layer as both the first and last layer is that, as a detailed analysis given later in the chapter will show, such a structure offers a slight improvement in the conversion efficiency.

The optimal performance of the transducer is obtained when the top electrode introduces no acoustic loading at the top layer of the ZnO.[1] The performance can be optimized by making the top electrode thickness much less than an acoustic wavelength or by making the thickness a multiple of one-half acoustic wavelength. The combination of the high frequencies and slow sound speed of the gold top electrode make it practically impossible to make electrodes that are substantially thinner than an acoustic wavelength. Using a high multiple of the acoustic wavelength is undesirable because the top electrode resonance will narrow the bandwidth of the transducer. A good compromise for the top electrode thickness appears to be between 1000 and 2000Å. Such thickness provided only small top electrode loading without reducing the bandwidth of the transducer to unacceptable levels. Gold is usually used as the top and counter electrodes because of its good conductivity and ease of vacuum deposition. In addition to the gold electrodes, a thin layer of titanium is usually used as an adhesion layer between the sapphire and the counter electrode, and a thin layer of chromium is used as an adhesion layer between the ZnO and the top electrode.
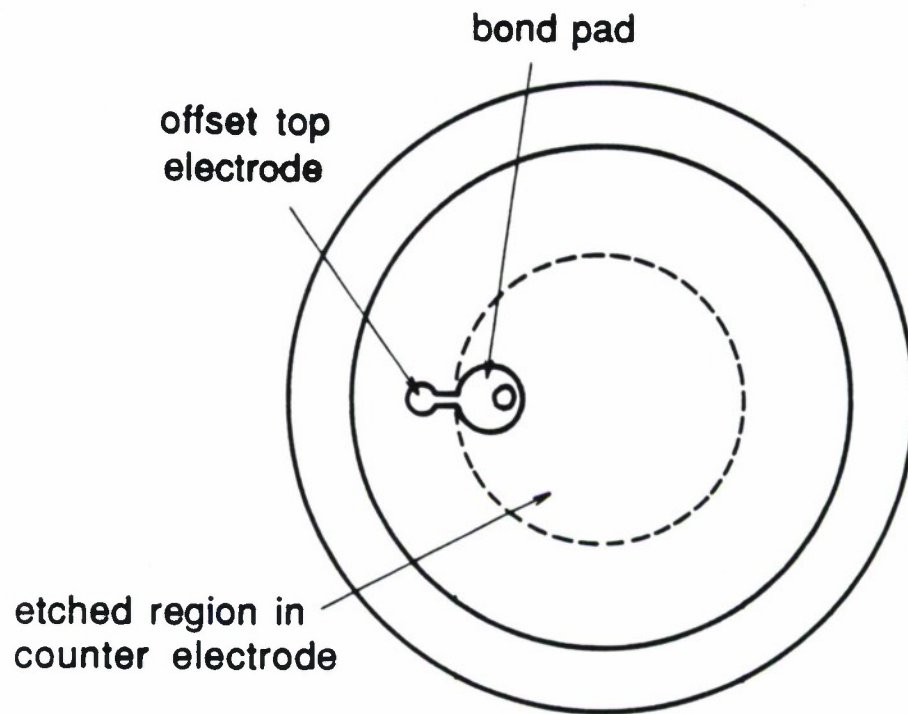
In most transducers, the top electrode is a circular metallic region which can be bonded directly with any of the standard thermo-compression techniques. Because of the expected conversion efficiencies in the millimeter-wave frequency range, the transducer radius is made as small as possible, only 20 μm, too small for direct bonding of the approximately 50 μm gold wire. Instead of bonding directly to the top electrode of the transducer, an "offset top dot" technique is used.[15] In the offset top dot technique, a hole is etched in the counter electrode before the ZnO is deposited. The top electrode is deposited as usual, but then instead of the circular top

dot normally used, a specially shaped top dot is deposited, Fig. 2.8. If the large bond pad is situated over the region without a counter electrode, it will not introduce significant capacitive loading. The transducer, on the other hand, is positioned over the counter electrode which completes the circuit. With the offset top dot technique, transducers with diameters smaller than the diameter of the gold ball bond can be used.
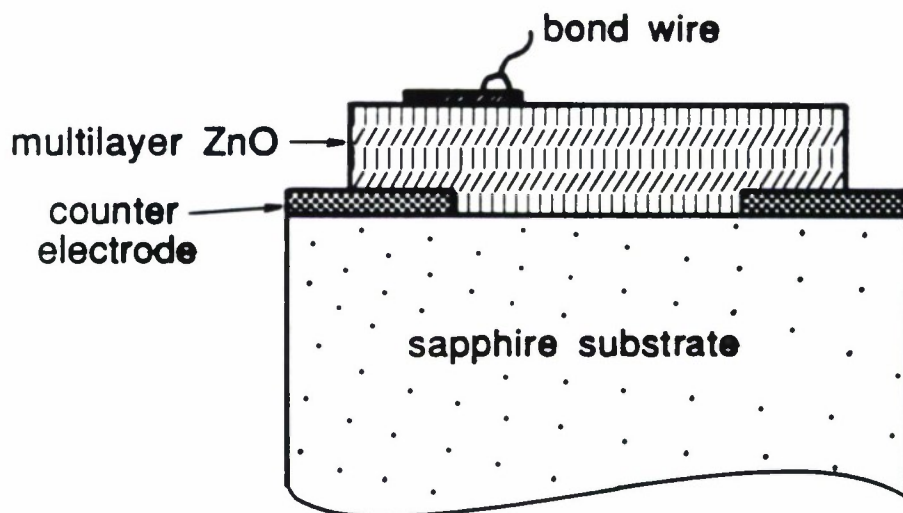
The transducers are mounted in a holder and the top electrode is connected to the microstrip line with a characteristic impedance of 50 Ω by pressing the 50-μm-diameter gold wire into some indium solder. The length of the gold wire is kept very short (typically less than 0.5 mm) to minimize the series reactance. In the Ka-Band, a coaxial connector at the other end of the holder is connected to the microstrip line and is used to bring the signals into and out of the transducer, Fig. 2.9(a). Because of the high loss encountered using coaxial connectors in the W-band, a transition between the WR-10 wave guide (characteristic impedance 400 Ω) and the 40 Ω microstrip line was constructed using a tapered reduced-height ridge-waveguide section[16], Fig. 2.9(b). The conversion efficiency of the transducer is measured using a pulse echo technique in which a short rf-tone burst is applied to the transducer and the resulting echo off the opposite end of the sapphire flat are measured. In order to improve the dynamic range of the measurements, a superheterodyne detection scheme in which the return signal is mixed down and detected at a lower frequency is employed.

(1) Verification of Theoretical Predictions

In the beginning section, it was stated that for most transducers it is the electrical response that dominates the conversion loss of the transducer. The validity of this assumption in this frequency range can be tested by changing the transducer configuration and measuring the conversion efficiency. If the conversion loss varies according to Eq. (2.2), the electrical losses are the dominant factor; if, on the other hand, the response deviates from Eq. (2.2) the acoustic losses must be considered in evaluating the multilayer transducer. The easiest way to modify the electrical conversion loss is to alter the real part of the transducer impedance, R_a. Because the capacitance of

bond pad

offset top electrode

etched region in counter electrode

(a)

bond wire

multilayer ZnO

counter electrode

sapphire substrate

(b)

Figure 2.8 Schematic of bonding to the transducer with the offset top dot technique.
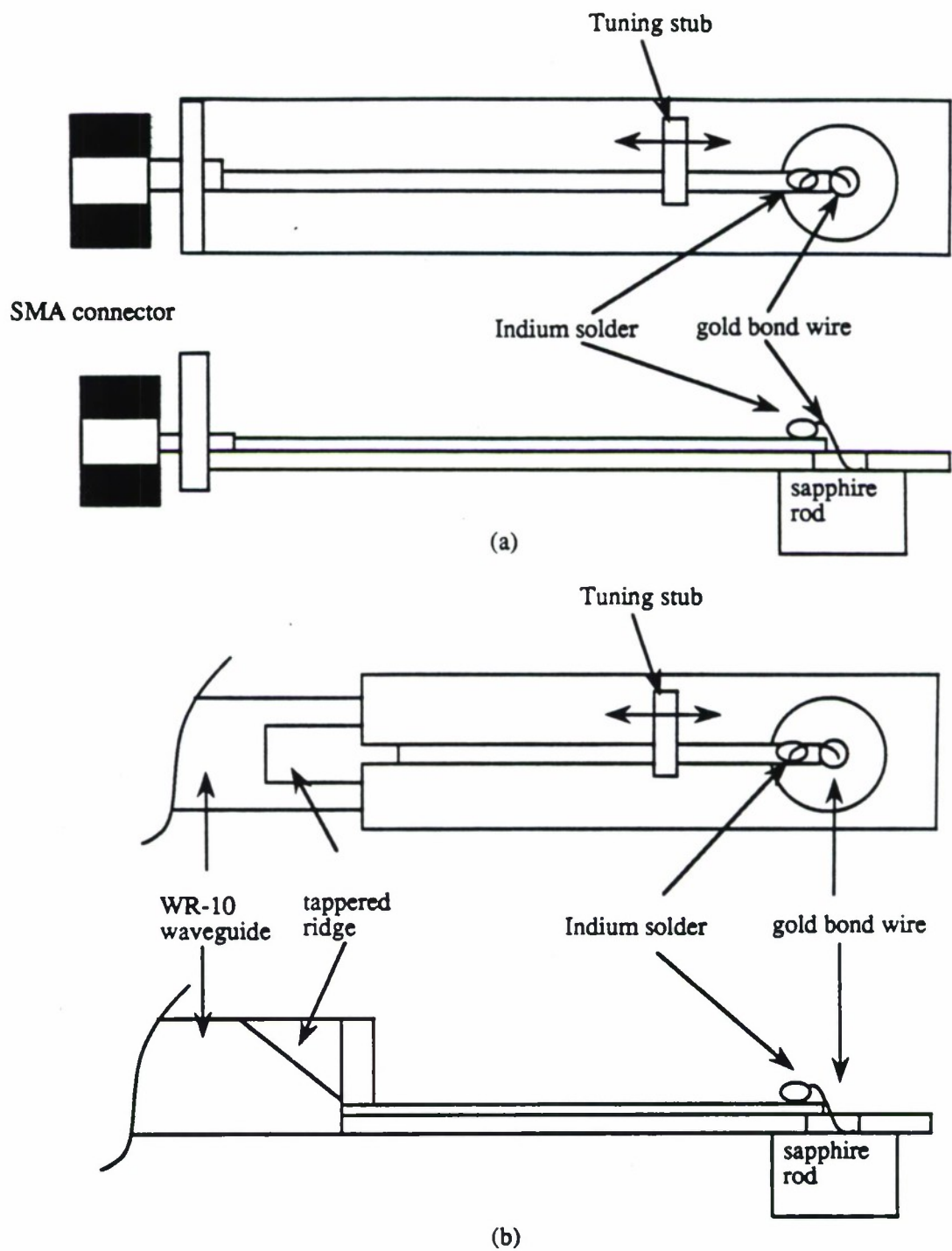(a) top view, (b) side view.

Figure 2.9 Electrical connections to the transducers.
(a) Ka-band, (b) W-band.

the transducer is proportional to the area of the transducer, R_a is most dramatically affected by changing the radius of the transducer.

In order to determine the effect of transducer radius on conversion efficiency, two transducers, both with offset top dots, were deposited on the same sapphire flat using the parameters described in Table 2.1.[17] The first transducer had a radius of 20 μm while the second

Total number of layers	15
ZnO layer thickness	950 Å
Top electrode thickness	1500 Å Ti/Au
Counter electrode thickness	1000 Å Cr/Au
Transducer radius	20 μm
Sapphire substrate thickness	2.6 mm

Table 2.1. Transducer parameters for Ka-Band transducers.

transducer had a radius of 60 μm. The highest conversion efficiency for both transducers occurred near 28 GHz with the 20 μm radius transducer having a "raw" conversion efficiency of 18 dB higher. The diffraction losses can be calculated to be 3.1 dB for the 20 μm radius transducer and 1.1 dB for the 60 μm radius transducer at 28 GHz. When the diffraction losses are subtracted from the data, the difference between the two transducers is 20 dB. Other minima can also be correlated between the two transducers. The minima near 30 and 35 GHz show a diffraction corrected conversion efficiency difference of 18 dB as shown in Fig. 2.10. If the conversion loss is calculated using Eqs. (2.2) and (2.4), the expected difference between the two-way conversion loss is 19 dB. This close agreement between theoretical and experimental values indicates that it is the losses in the electrical system, rather than the losses in the acoustic system, that dominate the untuned conversion efficiency.
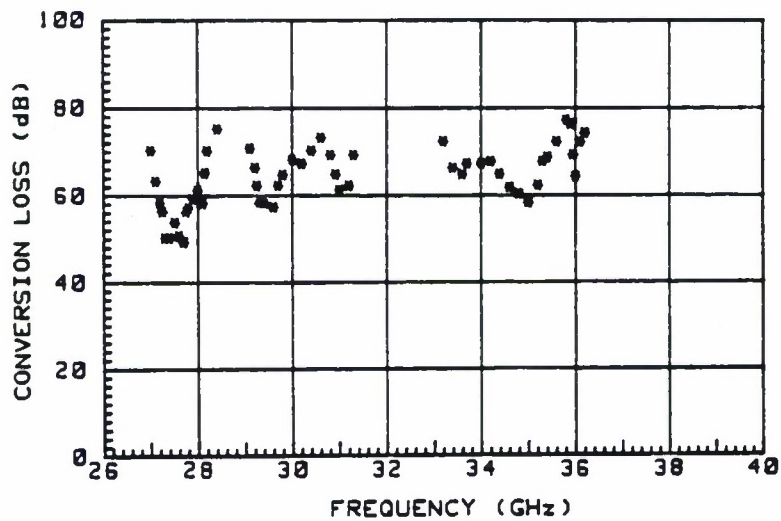
One of the conclusions that can be drawn from Eqs. (2.12) and (2.13) is that the transducers should operate at all the odd harmonics of the fundamental frequency. To test this prediction, one of the Ka-band transducers was operated in the the W-band to see if the transducer had measurable

TRANSDUCER RADIUS = 20 um
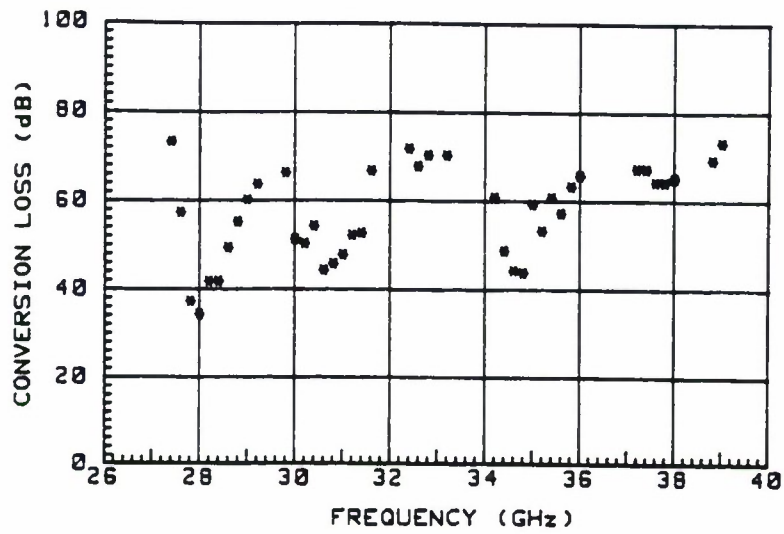
(a)

TRANSDUCER RADIUS = 60 um

(b)

Figure 2.10 Comparison of transducer radius on conversion efficiency.
(a) 20 μm radius transducer, (b) 60 μm radius transducer.

conversion efficiency at the third harmonic. Fig. 2.11 is a plot of the conversion efficiency in the W-band and, for comparison, a plot of the Ka-band response multiplied by a factor of three in frequency. The conversion efficiency at three times the fundamental Ka-band resonance is useful only in comparing relative responses as a function of frequency. As can be seen in the figure, the response at 28.6 GHz in the Ka-band is reproduced nicely by its third harmonic counterpart near 87 GHz.

Earlier work on single layer tilted ZnO films has shown that tilted ZnO transducers still had longitudinal wave coupling factors that were about half the magnitude of the normal ZnO value.[11] If each of the layers in the multilayer transducer has some longitudinal coupling, there will be some "bulk" response from the transducer near the half-wavelength resonance frequency for the whole transducer. Measurements were carried out on two of the Ka-band transducers in the 5-12 GHz frequency range to determine the bulk response. The conversion loss for the transducer mounted in hole number 4 is plotted in Fig. 2.12. The highest conversion efficiency is achieved around 9 GHz and is probably the second harmonic of the fundamental near 4 GHz. The bulk response of the transducer indicates that the value of $k_{bulk} = 0.21$.

Because the offset top dot technique had never been used at millimeter-wave frequencies before, its effectiveness with such short wavelength radiation needed to be evaluated. Two transducers were fabricated on the same substrate using the parameters in Table 2.1 except that the transducer radius was increased to 60 μm. One transducer had a circular top dot with the gold ball bonded directly to the top dot, the other had an offset top dot.[17] The two transducers had similar conversion efficiencies and frequency responses as can be seen in Fig. 2.13. This result suggests that the loading of the transducer by the gold ball and wire is probably a secondary effect and does not change the response of the transducer. It also appears that the effects of the unusual electrical connection used in the offset top dot technique are negligible at these frequencies even when the electrical wavelengths are only a few millimeters.
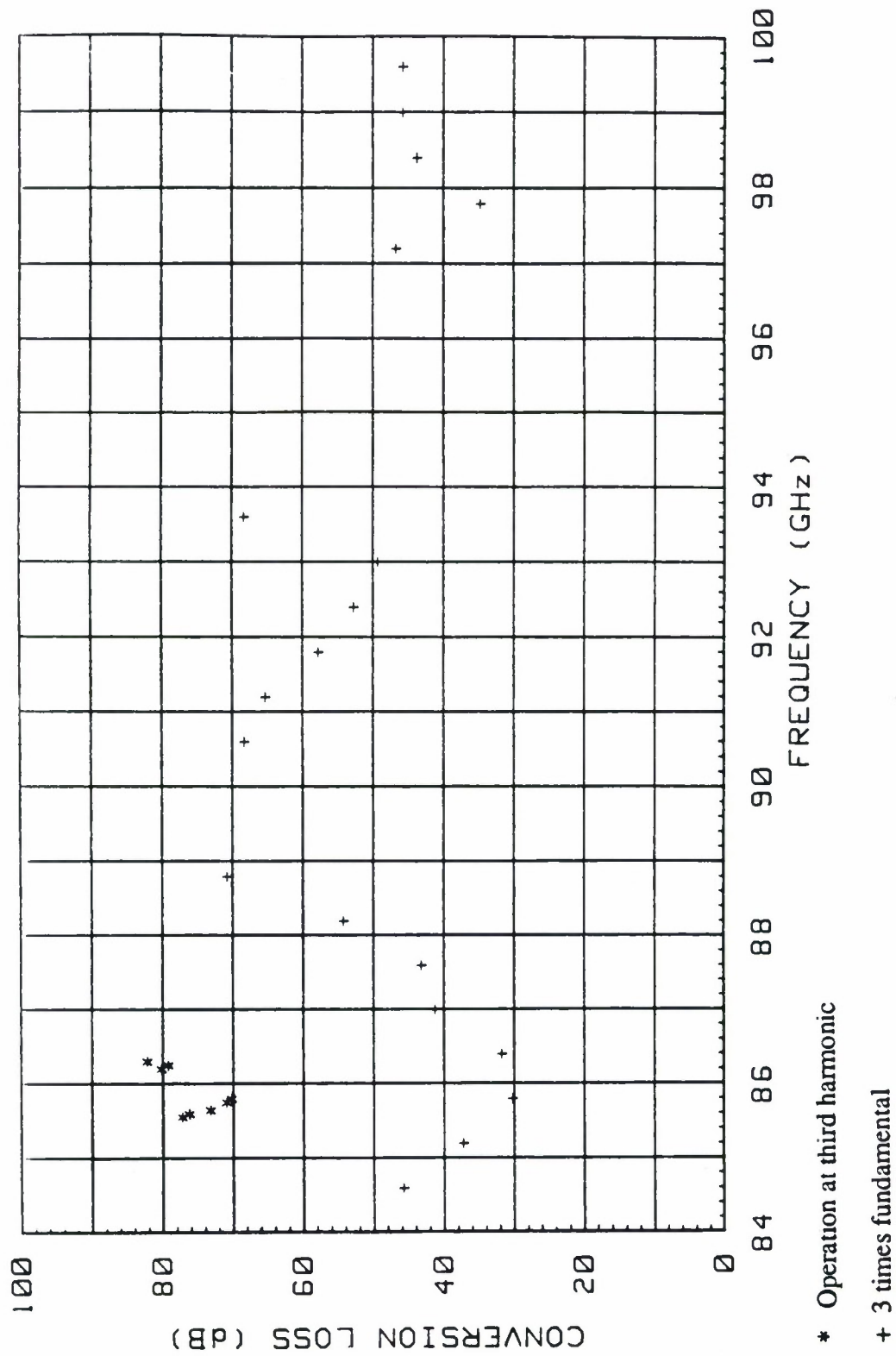
Fig 2.11 Frequency response of a multilayer transducer operated at the third harmonic.

* Operation at third harmonic

+ 3 times fundamental

25
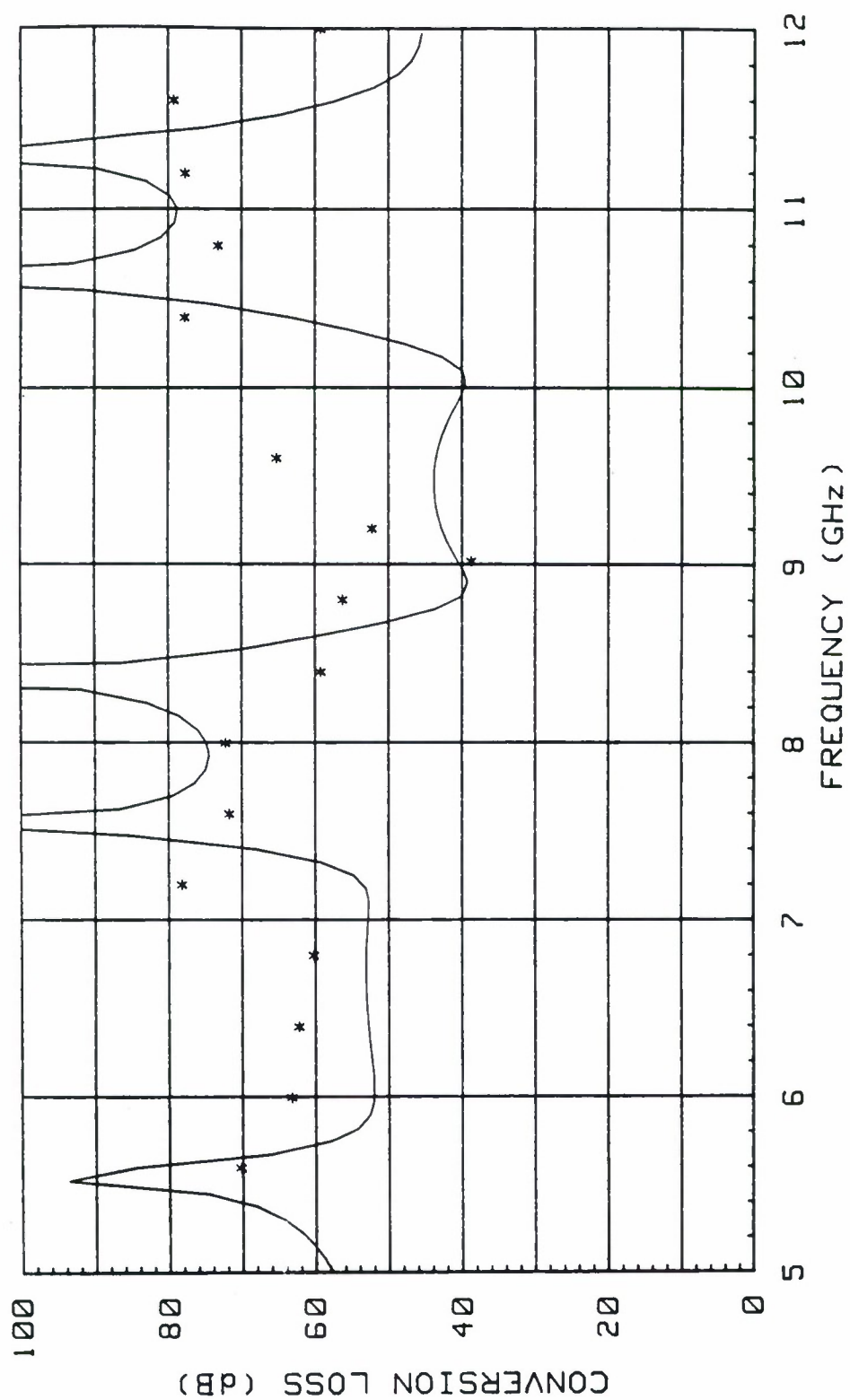
Figure 2.12 Bulk response of multilayer transducer.

26

GOLD WIRE BONDED TO 'OFFSET' TOP ELECTRODE
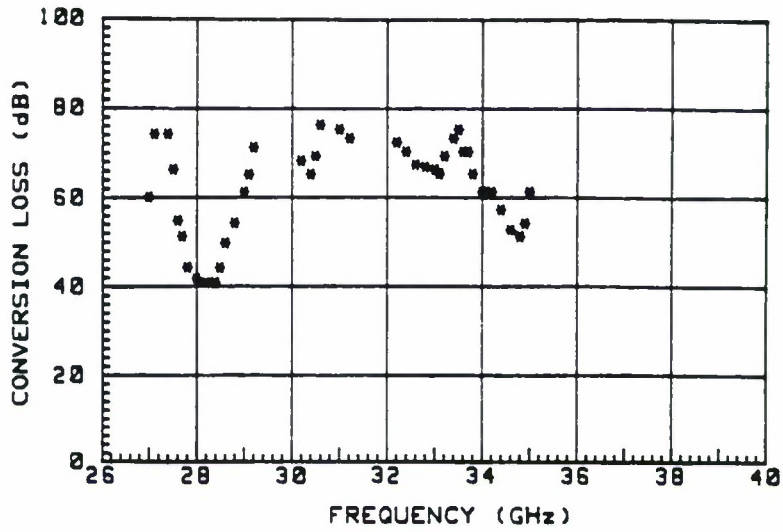
(a)

GOLD WIRE BONDED TO TOP ELECTRODE

(b)

Figure 2.13 Comparison of conversion efficiencies of the two top electrode bonding techniques.
(a) offset top electrode, (b) directly bonded top electrode.

27

4. Piezoelectric Modulation

The theoretical foundation for the multilayer transducer requires that there exist some periodic modulation of the piezoelectric constant in orde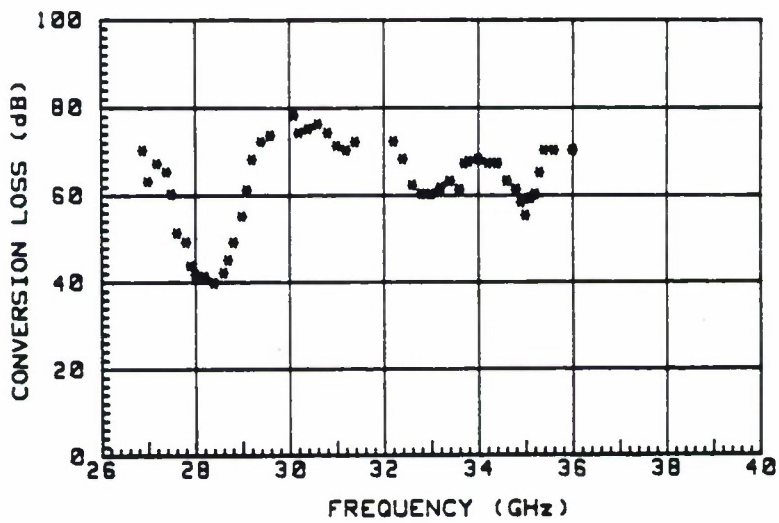r to achieve gain over the single layer transducer. The foundation for the multilayer ZnO transducer postulated that the normal and tilted layers would have a different orientation of the c-axis and thus a different piezoelectric coupling constant for longitudinal waves. Early work on films that were several microns thick had shown that the c-axis of the bulk crystal could be rotated by depositing the ZnO at a given angle.[13] It has been shown that the change in c-axis orientation does not occur abruptly but gradually changes over some finite transition distance.[18] If the distance required for the c-axis to change orientation is on the order of an acoustic wavelength, the theoretical approach used in Eq. (2.12) may not accurately model the physical situation. Additionally, an interface layer might necessitate changes in the thickness of either the normal or tilted layers in order to get the correct periodicity for maximum acoustic power generation. Experimental work on thin film tilted ZnO found that the films still had substantial longitudinal wave coupling even though the entire film was deposited at 40°.[11] The authors suggested that it was possible that, rather than having a "tilted" c-axis orientation as predicted, the film had more of an amorphous character. In order to more closely examine the grain structure of the layers and transition distance between crystal structure, the transducers were examined using electron microscopy.[19]

The transducers were first examined with the scanning electron microscope (SEM). The sapphire substrates were first cut from the back side to within 0.005 inches of the top surface. The remaining sapphire and the transducer were then cleaved by breaking the substrate along the cuts. This technique has proven effective in examining single layer transducers and seems to leave the exposed cross section free of debris and damage. The samples are then mounted and sputter coated with 100-200 Å of gold. The SEM micrographs of the multilayer structures reveal that every other layer of the transducer appears bright Fig. 2.14 (micrograph courtesy of Rosemarie Koch, Center for Materials Research, Stanford University). One possible explanation of the SEM micrographs is that the "normal" and "tilted" layers cleave at different angles yielding a "stair step"
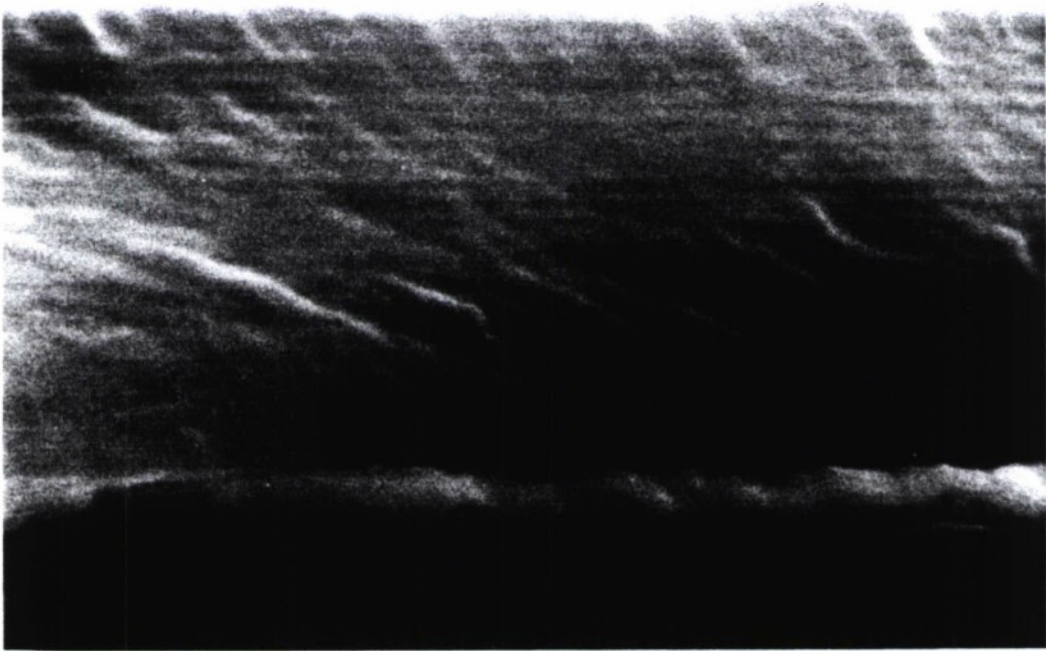
Figure 2. 14 SEM micrograph of a multilayer transducer.

topography that is imaged as bands by the SEM. In some high magnification images, the transition between the normal and tilted layer appears rather gradual and the transition between the tilted and normal layer seems sharper. Such transitions suggest that the change in the crystal axis orientation from a tilted film to a normal film may occur over a very short distance, but that the change in the c-axis orientation from normal to tilted layers occurs over a significantly longer distance. The SEM is unable to precisely determine the behavior of the interface between the layers because the sample must be coated with at least 100Å of Au to provide enough contrast.

In order to observe the interface between the layers without the gold coating, samples were prepared for examination using the transmission electron microscope (TEM). For the SEM samples, actual transducers whose conversion loss had been measured were imaged. Unfortunately, TEM thin film cross sections could not be made from films deposited on sapphire substrates because of the extreme hardness of sapphire. Silicon was chosen as the substrate for the TEM samples because other work had shown that high quality ZnO could be grown on silicon[20] and silicon was soft enough for use in TEM thin sections. Unfortunately, commerically available silicon wafers are so thin that acoustic measurements could not be performed on the transducers, so the conversion efficiencies of transducers examined with the TEM are unknown. The transducer sample was deposited on a Si wafer with a 1000Å thermal oxide. Because the sample did not need to resonate in a particular frequency band, convenient parameters were chosen for the deposition thicknesses as shown in Table 2.2.

Total number of layers	10
ZnO layer thickness	1000 Å
Top electrode	none
Counter electrode thickness	1000 Å Cr/Au
Substrate	Si with 1000 Å thermal SiO$_2$

Table 2.2 Parameters for the transducer examined by the TEM.

The TEM micrographs indicate the same banding structure as the SEM images but the individual layers can clearly be distinguished as seen in Fig. 2.15 (micrograph courtesy of Ann

100nm

Figure 2.15   TEM micrograph of a multilayer transducer.

Marshall, Center for Materials Research, Stanford University).   The banding is indicative of crystal changes between the normal and tilted layers. The TEM micrographs indicate that the "normal" layer is 1050Å thick, near the expected value of 1000Å. The "tilted" layers are 750Å thick, significantly less than the expected value of 1000Å. The error in the TEM measurement is less than ±5%. The discrepancy in the thickness of the tilted layer could come from several factors. The tilted layer may initially grow more slowly than the rate calculated using thicker film would indicate. It is also possible that some of the thickness attributed to the normal layer is deposited during the tilted deposition phase but its crystal structure more closely resembles the normal layer and is imaged as such by the TEM.

The TEM micrographs do not show the large scale changes in crystal grain structure between the normal and tilted layers that has been seen with thicker films.[9] Electron diffraction analysis of the TEM samples indicates that both the normal and tilted layers show strong c-axis orientation parallel to the surface normal indicating that the distance required for the crystal axes to change orientation is at least 750Å. The diffraction analysis also shows no significant differences between layers that were deposited at ± 40° to the surface normal. The small change in the c-axis orientation through the entire multilayer transducer indicates the c-axis orientation is not the major cause of the piezoelectric modulation. Even though the change in crystal orientation between the two layers appears small, the sharpness of the transition is still important because that will set an upper limit on the frequencies that can be generated using this method. Detailed examination of the interface between the normal and tilted layers indicates that the change in the TEM image contrast occurs over a distance of approximately 50 Å.

Another mechanism that could cause changes in the piezoelectric constant is differences in the chemical composition between the layers. A transducer with the same parameters as those in Table 2.2, with the substrate changed to sapphire, was examined using Auger electron spectroscopy. A depth profile through transducer is constructed by using argon ions to etch a hole in the sample while the Auger electrons from the region of interest are monitored. Using this method, a profile of elemental composition versus depth is created as shown in Fig. 2.16. The electron count rate can
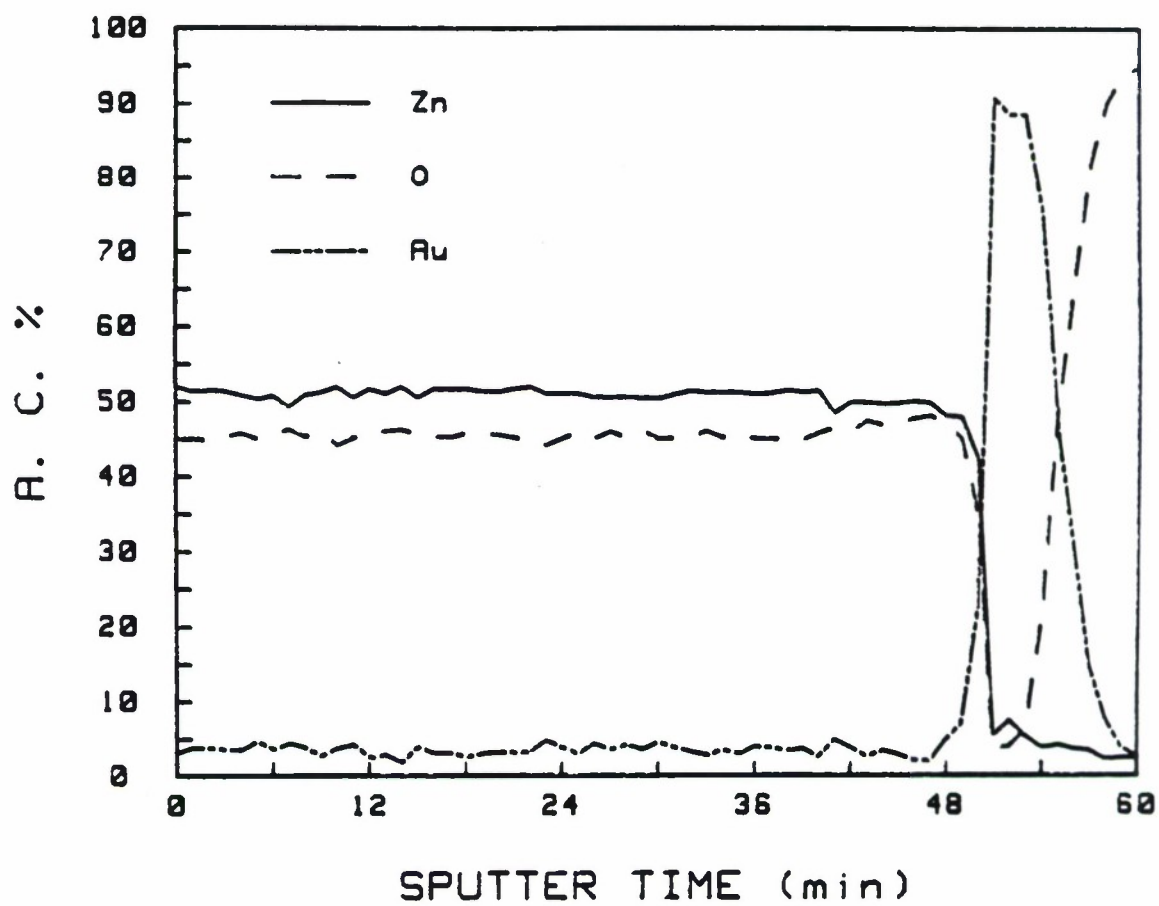
Figure 2.16 Depth profile of a multilayer transducer using Auger electron analysis.

then be calibrated against a sample of single crystal ZnO to determine if the layers vary in chemical composition. The spectroscopy reveals that there are no compositional changes that occur at the layer boundaries. The Auger analysis did yield one anomalous result; the first 2000Å of ZnO appears to be deposited with a higher oxygen concentration than the layers that are deposited afterward. The later layers have the same stoichiometry as single crystal ZnO. The abundance of oxygen present in the beginning of the deposition probably results from oxygen adhering to the surface of the Zinc target or excess oxygen adhering to the surface of the counter electrode. The higher oxygen concentration may degrade the performance of the transducer but should not interfere with the piezoelectric modulation.

5. Computer Simulations

The effects of various physical parameters on transducer performance have been investigated theoretically using a computer simulation based on the earlier work of Hadimioglu[3] and Sittig.[20] The multilayer transducer can be modeled by a Mason's equivalent circuit by making the following assumptions:

1) The transducer is considered to be one dimensional in the direction of sound propagation. The transducer radius is much larger than an acoustic wavelength and the electric and acoustic fields vary only in the thickness direction.

2) Each of the layers may have acoustic losses that vary as a function of frequency, but the losses in each layer must vary in an identical manner. The acoustic losses, α, must be small such that $\alpha << w/c$

3) Each layer is considered electrically lossless.

4) The top surface is approximated as a free surface and the substrate surface is approximated as a real impedance load.

5) Only the longitudinal acoustic modes generated in each layer are considered.

With the above assumptions, a series-connected multilayer transducer can be modeled by the Mason circuit in Fig. 2.17.[20] The following definitions are used in the Mason's model:
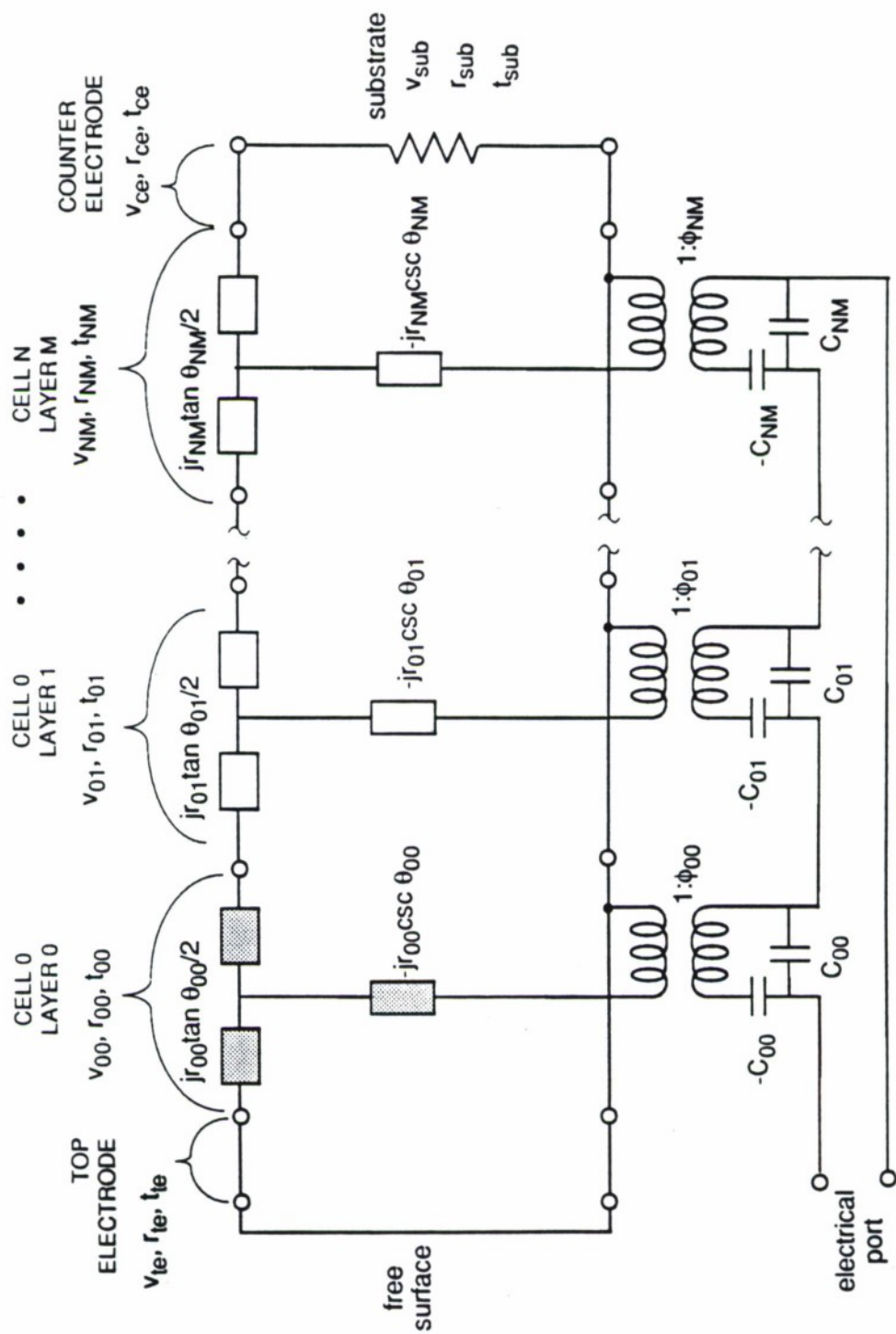
34

Fig 2.17 Mason's equivalent circuit for a multilayer transducer.

v   is the longitudinal sound velocity.

r   is the mechanical impedance.

t   is the layer thickness.

$C_0 = \dfrac{\varepsilon A}{t}$ is the clamped static capacitance of the transducer, where A is the area of the transducer and ε is the dielectric constant of the medium.

$\theta = \frac{ft}{v} + j\,\alpha(f)t$ is the propagation length in the medium, where $\alpha(f)$ is the loss in the medium which can be a function of frequency.

$\phi = C_0 h_{33}$ is the coupling constant of the medium, where

$$h_{33} = \frac{e_{33}}{\varepsilon_{33}^S} = k_t \left(\frac{c_{33}}{\varepsilon_{33}^S}\right)^{1/2}$$ is the piezoelectric coupling constant, e_{33} is the piezoelectric stress constant, ε_{33}^S is the permittivity at constant strain, c_{33} is the stiffness, and k_t is the electro-mechanical coupling constant.

the subscripts used in the Mason's model have the following meaning:

te   top electrode.

ce   counter electrode.

sub   substrate.

ij   layer j within cell i.

In the Mason's model, the current I, the voltage V, the force F and the displacement velocity U of one layer are related to the same quantities of the next layer by the following relation:

$$\begin{bmatrix} F_{n+1} \\ U_{n+1} \\ V_{n+1} \end{bmatrix} = [A_n] \begin{bmatrix} F_n \\ U_n \\ V_n \end{bmatrix} \qquad\qquad (2.13)$$

Because the layers are electrically excited in series configuration, the current I is the same for all layers. The components of the A matrix can be derived from elementary circuit analysis of the Mason's model in Fig. 2.17.

$$[A] = \begin{bmatrix} \cos\theta & -j\,Z\sin\theta & \dfrac{j\,h}{\omega}(\cos\theta - 1) \\[2ex] \dfrac{j\sin\theta}{Z} & \cos\theta & \dfrac{h\sin\theta}{\omega Z} \\[2ex] \dfrac{h\sin\theta}{\omega Z} & \dfrac{j\,h}{\omega}(\cos\theta - 1) & \dfrac{j}{\omega C_0}\left(\dfrac{C_0 h^2}{\omega Z}\cos\theta - 1\right) \end{bmatrix} \quad (2.14)$$

where ω is the angular frequency, Z is the impedance, C_0 is the clamped capacitance, and h the piezoelectric coupling constant. Each layer will have a different A matrix that depends on the material parameters for that layer. The A matrices for the top and counter electrodes can be created by setting their piezoelectric coupling constant, h, to zero.

Eq. (2.13) can be broken into parts so that the force F and the displacement velocity U can be solved iteratively.

$$\begin{bmatrix} F_{n+1} \\ U_{n+1} \end{bmatrix} = \begin{bmatrix} A_{11} & A_{12} \\ A_{21} & A_{22} \end{bmatrix} \times \begin{bmatrix} F_n \\ U_n \end{bmatrix} + \begin{bmatrix} A_{13} \\ A_{23} \end{bmatrix} \times I = [a_n] \times \begin{bmatrix} F_n \\ U_n \end{bmatrix} + [b_n] \times I \quad (2.15)$$

and thus:

$$\begin{bmatrix} F_{n+m} \\ U_{n+m} \end{bmatrix} = \left(\prod_{k=0}^{k=m-1} [a_k]\right) \times \begin{bmatrix} F_n \\ U_n \end{bmatrix} + \left\{\sum_{k=0}^{k=m-1}\left(\left(\prod_{l=k+1}^{l=m-1} [a_l]\right) \times [b_n]\right)\right\} \times I \quad (2.16)$$

where A_{ij} refer to the elements of the A matrix in Eq. (2.14). In this way, the forces and velocities at the top surface can be related to the forces and velocities at the counter electrode-substrate interface. The boundary conditions at these interfaces yield a set of simultaneous equations that are solved for the acoustic power radiated into the substrate.

Typical physical parameters used as input for the computer simulation are shown in Table 2.3.

Normal layer velocity	5800 m/s
Tilted layer velocity	5500 m/s
Normal layer coupling constant	.28
Tilted layer coupling constant	.21
Normal layer impedance	3.6×10^{-7}
Tilted layer impedance	3.2×10^{-7}
Top electrode velocity	2800 m/s
Counter electrode velocity	3100 m/s

Table 2.3. Transducers parameters used in computer simulation.

The values in Table 2.3 are derived from experimental and theoretical work done on single layer transducers at lower frequencies and provide a starting point for estimating the physical parameters at higher frequencies. In the simulation, the values of the various physical parameters and layer thicknesses are changed until a reasonable fit to the experimental data is obtained. Unfortunately, computer simulation using this model has yielded only satisfactory agreement with the experimental results, Fig. 2.18. The simulation does not consider several points that may have a bearing on the measured value. Because the program considers only the longitudinal wave propagation, the effects of any shear waves that may be generated in the "tilted" layers and the effects they have on the longitudinal waves generated in the "normal" layers is not addressed by the simulation.

Experimentally, no evidence of shear wave generation was found at powers 20 dB lower than the two-way longitudinal wave power in either the Ka or W-Band. If the effects of the shear waves are small, it should be possible to model the shear wave effects by modifying the velocity, impedance, and/or coupling constant of the tilted layer, but reasonable fits were obtained only when the estimated physical parameters differed greatly from their bulk values. It may be possible that while the shear wave power entering the substrate is small, shear waves play an important role in the longitudinal wave generation.
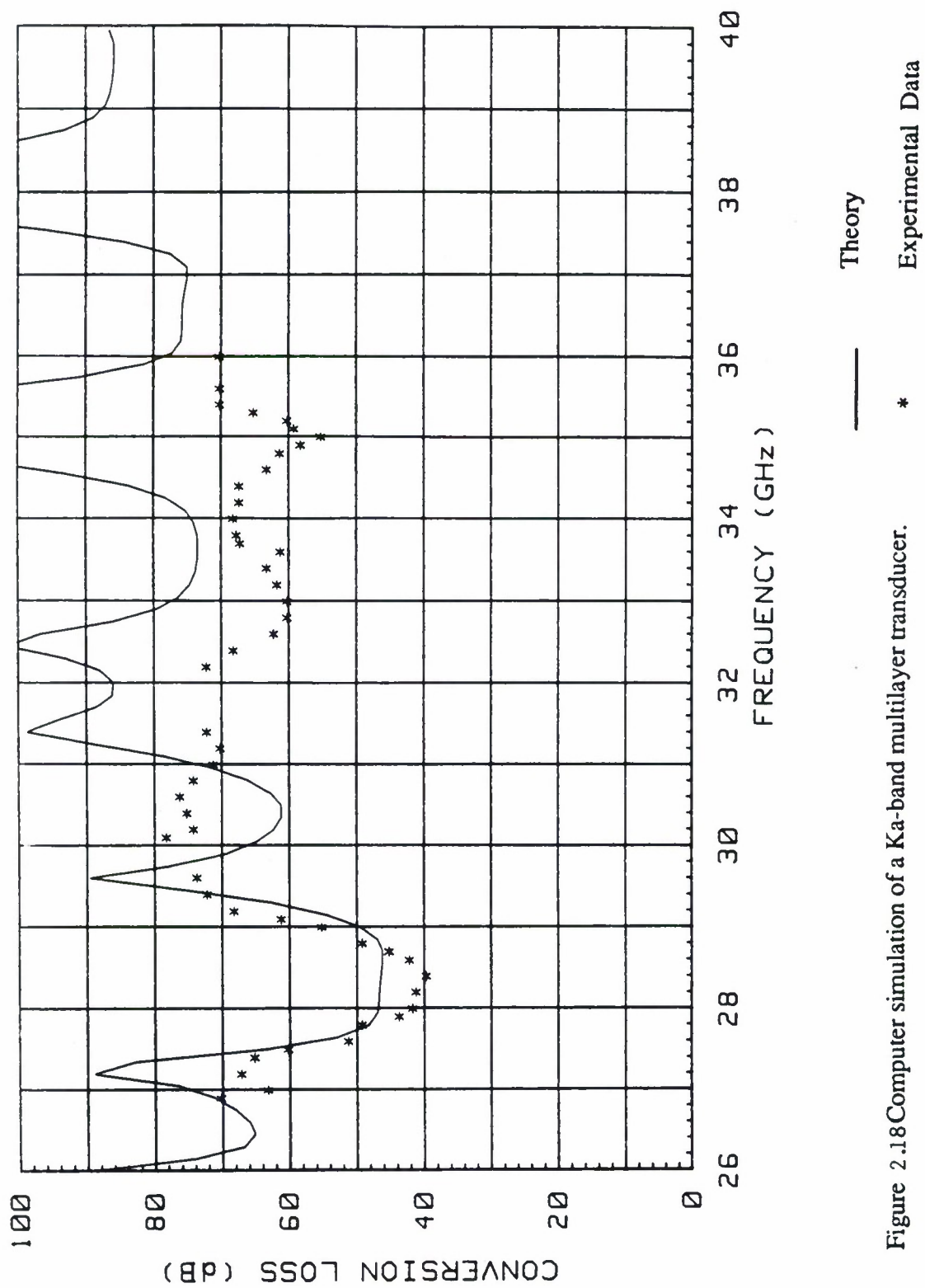
Figure 2.18 Computer simulation of a Ka-band multilayer transducer.

Theory ———   Experimental Data *

The simulation also assumes that each layer is uniform in crystal orientation and is identical to all the other layers of that orientation. While all the layers are deposited under nearly identical conditions, it is possible that the first normal layer which is deposited on gold could have different physical properties than the other normal layers which are deposited on tilted ZnO. The use of both positions II and III for depositing the tilted ZnO may result in some differences between the tilted layers. Several simulations were run with different physical parameters for the ZnO layers deposited in position II and III, but good agreement with the experimental data required highly atypical values.

Another aspect of the multilayer transducers that has been difficult to model is the transition region between the normal and tilted layers. The TEM analysis indicated that the distance between the ZnO crystal structures occurred over a short distance, but the interface layer could still play an important role in the longitudinal wave generation. Two methods have been used to simulate a small transition region between the layers on the computer. The first method assigned the transition region to one or the other of the layers and used the physical properties of the assigned layer for the transition layer. The second method involved modeling the reorientation region as a thin layer between each of the two larger layers. The physical parameters of the transition region were computed to be the arithmetic mean of the layers on either side. Neither approximation yielded significantly better agreement with experimental data than simply omitting the transition region altogether.

6. Extension to Higher Frequencies

In the past, coherent millimeter-wave frequency acoustic wave generation has been accomplished at frequencies as high as 114 GHz by placing a quartz crystal in the high electric field region of a cavity.[21] Because the W-band multilayer ZnO transducers have a conversion loss that is typically 50 dB less than the quartz transducers, it is useful to examine the possibilities of operating the ZnO multilayer transducers at even higher frequencies. Several practical problems must be overcome if the higher frequency transducers are to be constructed and evaluated. The acoustic attenuation in sapphire at higher frequencies must be considered, and while no one has

40

measured the acoustic attenuation of sapphire millimeter-wave frequencies higher than 100 GHz, results on quartz indicate that unless the sample is cooled to below 20 K the acoustic attenuation may pose a serious problem.[21] The W-band multilayer transducers have been operated at temperatures as low as 2 K without any damage to the transducer indicating that the transducers can be cooled to very low temperatures to reduce the attenuation if necessary. Cooling the sample should also reduce the acoustic attenuation in the ZnO, leading to higher conversion efficiencies.

Another major problem is that the current pulse echo detection technique places extremely tight specifications on the parallelism and flatness of the sapphire substrates. Any surface irregularities or imperfections on the substrates will also place an upper limit on the operating frequency that can be detected using this technique. In the W-band, the non-flatness and non-parallelism of the sapphire substrate were already affecting the measurements. At 300 GHz, the wavelength of sound in sapphire will be about 350 Å and would require extremely high tolerances on the sapphire. Even if the transducer radius is as small as 20 μm, the sapphire substrate would still have to be flat to within 3 μm over the 1/4" diameter of the sapphire rod to ensure destructive interference did not completely destroy the incoming signal.

One way to overcome the substrate problems is to detect the signal with some type of incoherent detector which would not be as sensitive to the substrate condition. Other researchers have shown that if the sound can be coupled from the substrate into superfluid helium under the right conditions, the helium is capable of propagating the 200 GHz sound for distance of millimeters.[22] Using this approach, the detector could be located at some distance to decrease any rf coupling between the transducer and detector.

Several problems also confront the transducer design if the frequency range is to be increased. One of the problems that may be encountered in extending the operating frequencies above 100 GHz is maintaining the periodicity in the piezoelectric modulation. In a non-ideal transducer, the layer thicknesses are going to be distributed around one-half wavelength because of variations in the deposition parameters. One can estimate the effect of thickness variations on the output power. If the separation between active layers is not exactly one acoustic wavelength, the

wave produced in that layer will have some phase offset relative to the entering wave. The acoustic amplitude at the substrate would then be:

$$A_{ac} \propto A_0 \sum_{n=1}^{N} e^{i\phi(n)}$$

(2.17)

where A_0 is the acoustic amplitude generated at each interface, and $\phi(n)$ is the phase difference between the "ideal" wave and the acoustic wave generated at the boundary between the layers. If N is large, Eq. (2.17) can be approximated by:

$$A_{ac} \propto A_0 N \int_{-\pi}^{+\pi} P(\phi)\cos(\phi)d\phi$$

(2.18)

Where $P(\phi)$ is a weighting function describing the distribution of ϕ. If $\phi(n)$ is randomly distributed about 0 such that $-\theta \leq \phi \leq \theta$,

$$P(\phi) = \begin{cases} 0, & \phi < -\theta \\ \dfrac{1}{2\theta}, & -\theta \leq \phi \leq +\theta \\ 0, & \phi > +\theta \end{cases}$$

(2.19)

Substituting Eq. (2.19) into Eq. (2.18) and integrating yields:

$$A_{ac} \propto A_0 N \frac{\sin(\theta)}{\theta} = A_0 N \, sinc(\theta)$$

(2.20)

The effect on the power radiated into the substrate can be estimated by expanding $sinc^2(\theta)$ in a Taylor series about $\theta = 0$.

$$\text{sinc}^2(\theta) = 1 - \frac{2}{3!}\theta^2 + \left[\frac{1}{(3!)^2} + \frac{2}{5!}\right]\theta^4 - \dots \tag{2.21}$$

If θ is small, then to first order, the power entering the substrate will be unaffected by the thickness variations. A good estimate for θ can be found by estimating the error in the thickness caused by variations in the deposition rate and time for each layer. The error in the deposition is probably limited to a few monolayers of ZnO or about 20Å. For transducers operating in the Ka-Band, the acoustic wavelength in ZnO is approximately 2000Å and $\theta = 7.2°$, yielding a two-way decrease in power of only 0.05 dB. For transducers operating in the W-Band, the effect is more pronounced, but still small. The typical wavelength in the W-band is approximately 600 Å and $\theta = 24.0°$, resulting in a two-way power loss of 0.5 dB. The two-way conversion efficiency would not be reduced by 10 dB until the acoustic wavelength reaches 150 Å or about 350 GHz.

The minimum distance required to modulate the piezoelectric constant between the layers will also determine the maximum operating frequency of multilayer ZnO transducers. If the piezoelectric constant changes over the same region as the TEM image contrast, about 50 Å, it should be possible to deposit transducers with layers as thin as 100 Å, corresponding to operating frequencies of about 300 GHz, and still achieve reasonable conversion efficiencies. Because the output power increases as the number of layers squared, it is also possible that the number of layers could be increased by an order of magnitude or more to generate sufficient power at higher frequencies.

In conclusion, multilayer ZnO acoustic transducers have been designed and tested at operating frequencies from 24 GHz up to 100 GHz. These transducers are by far the most efficient transducers in this frequency range ever constructed. These transducers offer the possibility of designing a superfluid helium acoustic microscope with a resolution as high as 30Å. It also appears that multilayer ZnO transducers can generate coherent phonons at frequencies as high as 300 GHz with reasonable conversion efficiencies. Although some features of the transducer's performance cannot be accounted for by computer simulations, the transducer's

performance closely matches the theoretical predictions regarding harmonic generation and dependence on transducer radius.

III. Propagation Studies in Liquid Helium

Liquid helium cooled below the Lambda point is a suitable media for propagating sound at the frequencies of interest in this report and it is important to increase our understanding of the linear and nonlinear properties of this liquid. The non-linear properties were investigated with a spherically converging acoustic beam. Since the power densities are very high at the focus, the nonlinear effects are enhanced, particularly as the frequency is increased. The use of very low temperatures prevents scattering by thermal phonons, but the signal-to-noise ratio is limited by the onset of noise-stimulated nonlinear scattering. This three-phonon process, which becomes stronger as the frequency increases, produces an effective attenuation as it absorbs power from the fundamental frequency of the signal beam. This "attenuation" can be greatly decreased, and thus the signal-to-noise ratio increased, simply by applying pressure to the helium bath.

1. The Three-Phonon Process

Figure 3.1 depicts a three-phonon scattering event in which two phonons collide and form a third phonon (the reverse process also occurs). The collision conserves energy and momentum. The phonon energy is hf, where f is the frequency and h is Planck's constant; thus conservation of energy requires $f_1 + f_2 = f_3$. The phonon momentum is $hk/2\pi$; thus conservation of momentum requires $k_1 + k_2 = k_3$. If the dispersion were linear, i.e., $f=ck/2\pi$ for all frequencies (where c is a constant speed of sound), then the two conservation equations require that the phonons be collinear--all momenta in the same direction. If the dispersion is upward, as shown in the figure, then the sound speed c is increasing with frequency. Thus the higher energy phonon f_3 will have less momentum than the dispersionless case. The two input phonons must then intersect at a finite angle so that some of their momentum will be cancelled and the momentum can be conserved (the drawing in the figure depicts this upward dispersion case). If the dispersion is downward, however, the higher energy phonon has too much momentum (more than can be obtained from the
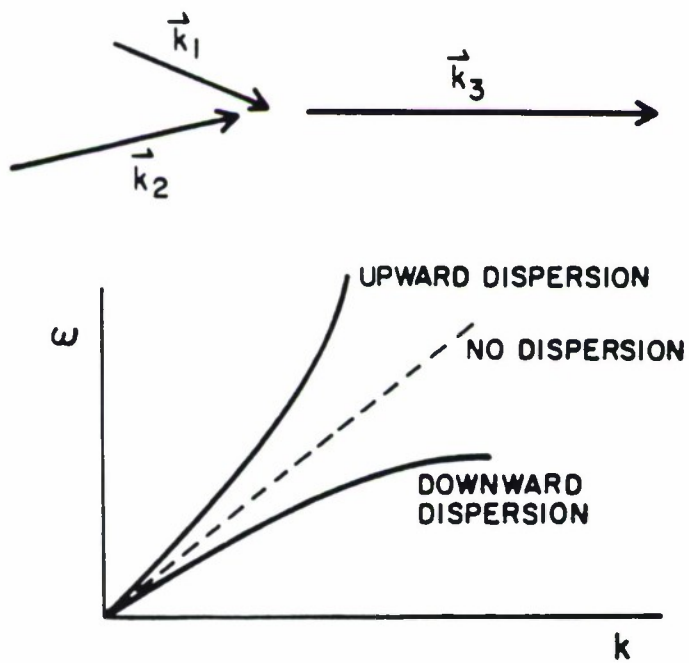
FIGURE 3.1 Diagram showing the scattering of two phonons to form a third for various dispersion cases.

two smaller phonons) so that momentum cannot be conserved. Downward dispersion thus makes the three-phonon process much less likely.

It must also be pointed out that when the dispersion is linear, the three-phonon process that dominates is not the difference frequency process, associated with gain, but the sum process, associated with the formation of higher harmonics, and, in normal liquids, a shock wave. Studies of harmonic formation have been made for focused acoustic beams in cryogenic liquids.[23]

The three-phonon process is frequency dependent, with an effective attenuation that goes as the *fifth* power of frequency.[24,25,26] Even worse, once a scattering event occurs in which the beam phonon is scattered into two smaller phonons, these products are exactly phase-matched with all the other signal phonons to scatter them, in an avalanche-type process, as demonstrated through experiments using plane waves.[27] In optics, the stimulated amplification of spontaneous decay products has long been understood. It was first demonstrated in visible light by Akhmanov *et al.*,[28] Magde and Mahr,[29] and Harris *et al.*[30,31,32] In the last experiment, for example, just by shining a high frequency beam onto a lithium niobate crystal the spontaneous decay products could actually be amplified up to where they were visible with the unaided eye. In the acoustic experiments, Foster and Putterman[27] showed that the process could go on in the higher nonlinearity of the helium until the input beam ("pump") is actually depleted by more than 30 dB.

Thus, unless something is done to limit this mechanism, it would be nearly impossible to construct a very-high-frequency acoustic microscope. The signal would deplete too rapidly at higher frequencies (though at extremely high frequencies the dispersion is downward at all pressures, as shown by the millimeter path lengths of 10-20 Å phonons).[33] Fortunately in superfluid helium the dispersion is adjustable. At low pressures, the dispersion is upward, and so the three-phonon collision occurs at a finite angle. As pressure is applied the dispersion becomes more linear (collision angle becomes smaller), and finally, above 18 or 20 bar, the dispersion turns downward. With the dominant scattering process thus forbidden, the fluid should be much more transparent for sound waves at helium bath pressures above 20 bar, and the microscope should have a higher signal-to-noise ratio.

At this point it is important to understand the difference between nonlinearity and dispersion. Nonlinearity is dependent on the INTENSITY of the beam and gives the relative coupling or interaction between different modes. Dispersion is dependent on the frequency of the mode, and describes whether or not that interaction grows as the beam propagates (or, in other words, whether momentum is conserved).

2. Experimental Results Using a Focused Beam

To study these nonlinear effects at high power densities an acoustic lens and a reflector were placed in a pressure cell (Fig. 3.2). The cell has been described previously.[34] The cell allows the lens-sample spacing to be adjusted while varying the pressure applied to the fluid from saturated vapor pressure (a very good vacuum) up to 26 bar, above which the liquid helium freezes. The experiment measured the intensity of sound pulses which bounce off the reflector (polished, flat sapphire) and return to the acoustic lens. The received signal is plotted in Fig. 3.3 as a function of pressure in the cell for two frequencies with two different acoustic lenses. It can be seen that although the shape of the curve is considerably different between the two lenses (believed to be due to slight variations in the shape of the foci caused by slight variations in the illumination of the lenses by the transducers) there is a 20 dB increase in the signal-to-noise ratio near 20 bar.

A study was also made of the effects of very high power densities at various pressures using the 8 GHz lens and flat.[35] Plots of the output power as a function of input power at various pressures are shown in Fig. 3.4, where the input power has been rescaled in terms of the Mach number, given as:

$$M = \sqrt{\frac{2I}{\rho_0 c_0^3}} \qquad (3.1)$$

where ρ_0 and c_0 are the density and speed of sound, respectively, of the helium, and I is the intensity of the sound beam (all the signal power is assumed to fall on a spot which is diffraction-
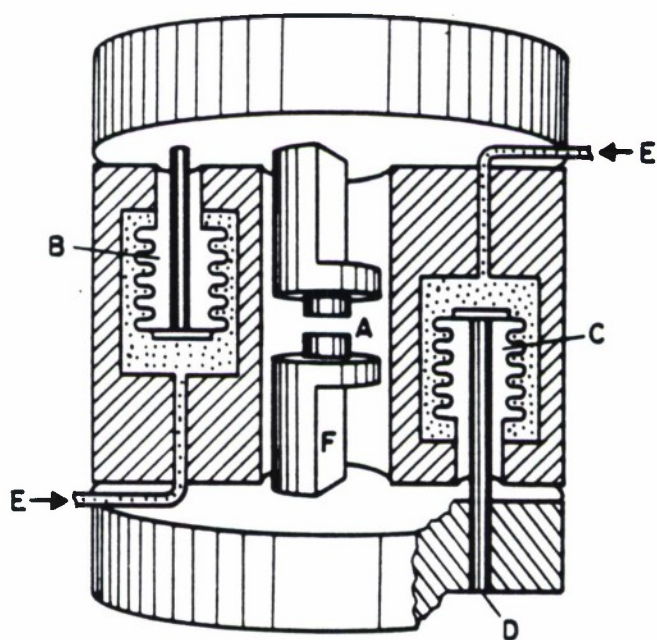
FIGURE 3.2 Cutaway view of the pressure cell, showing
(A) Sapphire rods for lens and flat reflector, (B) and
(C) Miniature bellows, (D) Pushrod, (E) Control
capillaries, and (F) Impedance-matching circuitry.
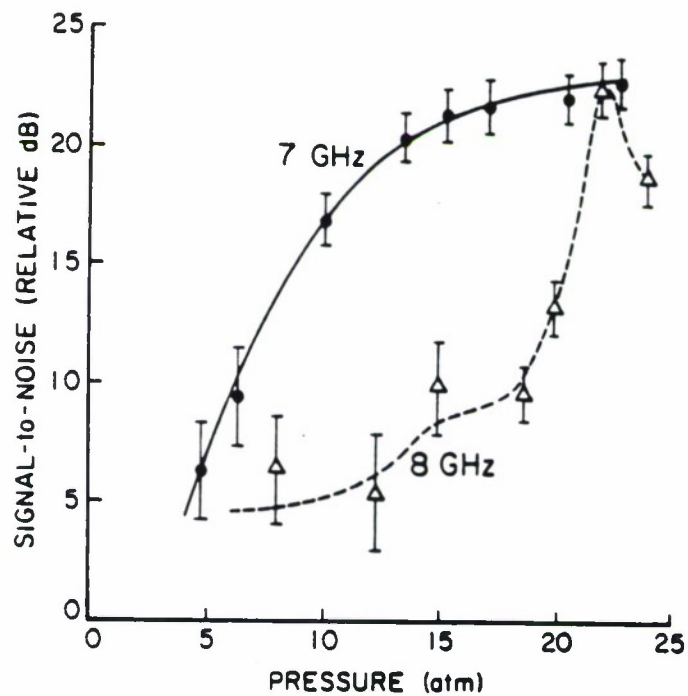(from Reference 12).

FIGURE 3.3 Improvement of the Signal-to-Noise ratio upon
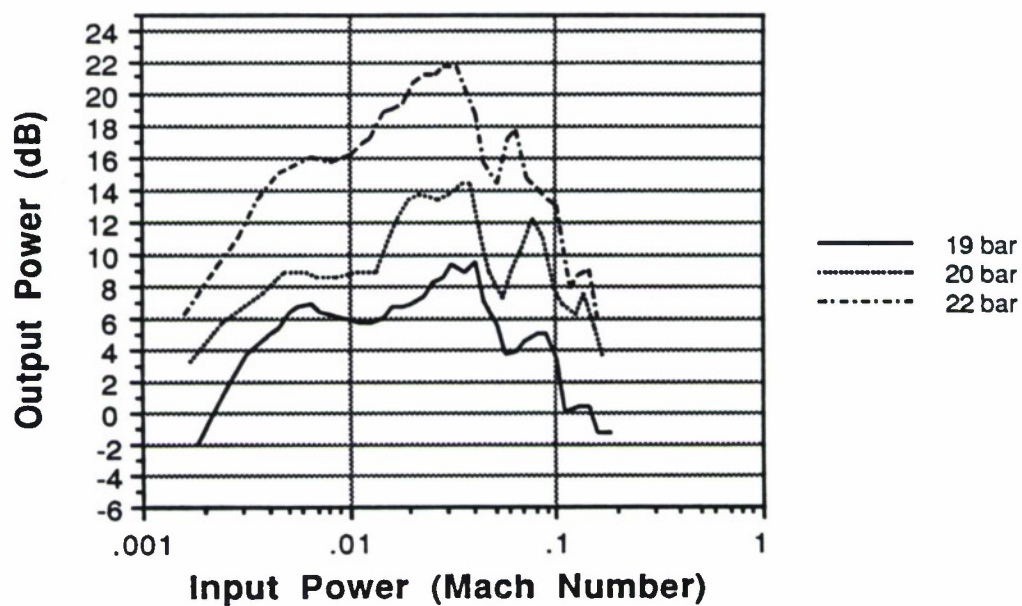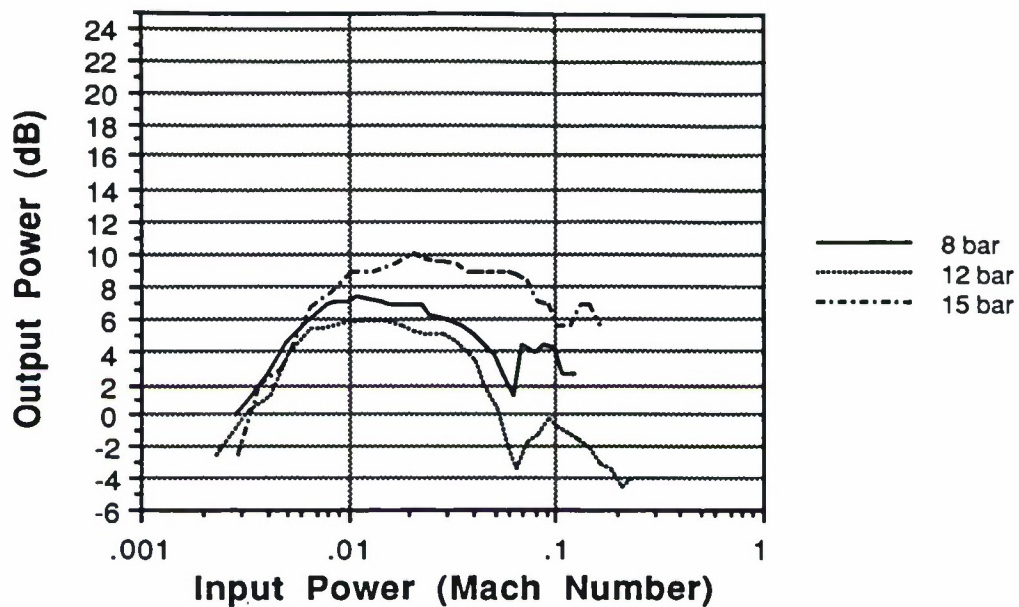pressurization of helium at frequencies of 7 and 8 GHz.

FIGURE 3.4 Power received (0 dB corresponds to the noise level of system) as a function of input intensity, given as Mach number at focus, for various bath pressures.

limited with diameter of one wavelength times the f-number of the lens). Three regions of pressure with different behaviors are observed. Each of these three regions will be discussed in turn.

At low pressures, 8 bar and 12 bar, the dispersion curve is upward, or "anomalous," that is, the speed of sound increases with increasing frequency.[36] Spontaneous decay of the signal is thus possible using a three-phonon process (3pp) where the decay products have frequencies ω_1, ω_2 and wavenumbers $\mathbf{k}_1$, $\mathbf{k}_2$ satisfying

$$\omega_1 + \omega_2 = \omega_p; \mathbf{k}_1 + \mathbf{k}_2 = \mathbf{k}_p \qquad (3.2)$$

where the subscript p (=pump) refers to the input signal. The beam can thus spontaneously decay into two noncollinear phonons. Pump depletion is the result of parametric amplification of the stimulated decay products. Such behavior has already been reported for plane waves in superfluid helium.[27]

At an intermediate pressure, 15 bar, the dispersion is almost linear. As the dispersion gets more and more linear, the available angle between the decay products gets smaller and smaller. Hence the sum processes should dominate. That is, the phonons in the beam are more likely to scatter off each other to produce harmonics than to scatter off the noise to decay. The beam power thus saturates. The power remains constant over a 15 dB range in input power.

At high pressures, 19 bar, 20 bar, 22 bar, the dispersion curve is downward, so that neither the three-phonon decay nor harmonic formation is phase-matched, that is, conserving both energy and momentum. As one adds increasing amounts of power to the system, however, the output, rather than saturating, continues to rise to a much higher signal level. Then as more power is added, the output level actually *decreases*. The pump is then experiencing more than the simple saturation that might be expected in shock wave formation, where additional energy is simply transferred into harmonics. A decrease in output with additional input would seem to be due to one of two causes. Either there is a major alteration in the nature of the medium, or there is a stimulated process occurring, in which phase-matched decay products are parametrically amplified at the expense of the pump. Each will be discussed in turn.

51

3. Analysis of Data

A number of other effects associated with high-intensity sound propagation in liquid helium might alter the medium and account for the results at high pressure, namely cavitation, streaming, vorticity, and rapid melting and freezing. Above a certain critical amplitude, cavitation can result in massive signal loss. There was not, however, any increase in noise associated with cavitation and bubble collapse,[37,38] even using a spectrum analyzer. Also, evidence from another system indicates that at higher frequencies the cavitation amplitude increases linearly with frequency,[38] and extrapolation from helium experiments imply a much higher threshold than even the intensities used here.[39] On the other hand, the present amplitudes *are* larger than the onset for streaming reported in helium.[40] Streaming, however, is an effect usually associated with continuous sound, while here the pulses were short and the duty cycles low. The returned signal strengths were also independent of the pulse width and repetition rates. Furthermore, observations using a spectral analyzer showed no spectral (Doppler) shifts within the roughly 100 MHz bandwidth of the lens-amplifier system. Another possible effect is that the intensity at the focus could be high enough to cause a small section of the superfluid to go "normal," due to the high vortex density. This process should be a slow one.[41] Experiments using multiple pulses showed, however, that the pulses were completely independent-noninterfering on time scales as short as 100 nanoseconds. A final alternate explanation is rapid melting and freezing of the helium at the focus. This process is very fast, occurring at even gigahertz rates.[42] However, the output was stable in time, and showed no abrupt change with increased helium bath pressure, as might be expected from a phase change. Rather, it showed a slow progression between the various regimes of pressure.

Since there are reasons to discount the helium-altering effects, the possibility of a stimulated process must be considered. At high pressures the simple three-phonon process above cannot conserve both energy and momentum. The next simplest decay process which *can* conserve both is the four phonon process in which two pump phonons scatter:

$$\omega_1 + \omega_2 = 2\omega_p; \; \mathbf{k}_1 + \mathbf{k}_2 = 2\mathbf{k}_p \tag{3.3}$$

Referring back to Fig. 3.4, one also notices that the rate of drop of output signal with increasing input signal is twice as steep as that for low pressures. This result is consistent with Eqs. (3.2) and (3.3), since now two pump phonons are consumed in each stimulated decay event, versus one for the three-phonon process. Spontaneous decay (also called *parametric noise*) via four-photon processes has been observed in optics.[43,44] We believe these data to show the first observation of such a phenomenon in acoustics.

This conclusion regarding the interpretation of the collinear gain observed in the parametric amplifier should be adjusted slightly. The probable interaction is, like that one, between four phonons, but as a two-step process of two non-momentum-conserving three-phonon processes.

IV. The Parametric Amplifier Experiment

Studies of nonlinear acoustic interactions in superfluid helium at temperatures below 0.2° K have culminated in the construction of an all-acoustic parametric amplifier at gigahertz frequencies. This device represents the shortest wavelength parametric amplifier ever made, with signal wavelengths shorter than 1000 Angstroms and pump wavelengths shorter than 600 Angstroms. In the experiment, plane waves are mixed at a predefined angle in the superfluid helium. Two gain regimes are observed. The first regime is a noncollinear phase-matched process, in which the signal phonon stimulates decay of the pump phonon to create gain at the signal frequency. The second regime is a four-phonon collinear process, in which gain on the signal is created by the second-harmonic of the pump. This four-phonon process is unusual and is shown to be a combination of three-phonon processes wherein the lack of conservation of energy and momentum in one process is mostly compensated by the other.

1. The Plan

The experimental geometry is depicted in Fig. 4.1. The pump and signal phonons are launched from a sapphire substrate into liquid helium at an angle determined by the dispersion in helium and the frequencies of the pump and signal waves. The signal phonons are amplified and
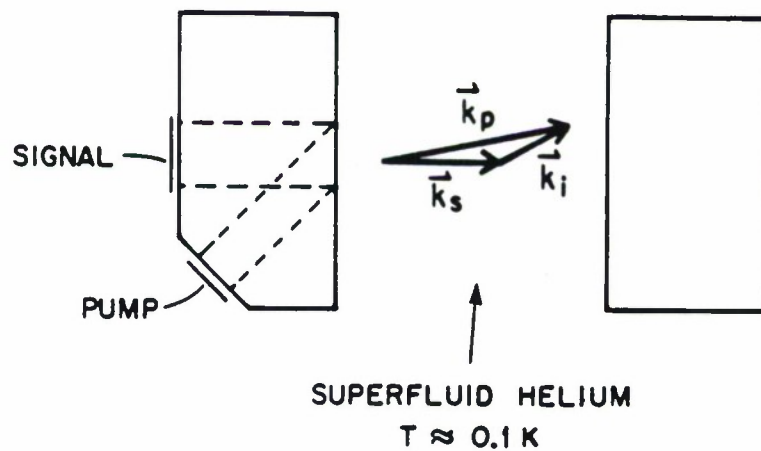
FIGURE 4.1 Experimental geometry of Parametric Amplifier experiment in superfluid helium. The "bottom crystal" (right) reflects the beam back, or else a third transducer can be deposited on its backside.

detected, either (after reflection) by the transmitting transducer, or by a third transducer on the other flat.

To determine which frequency pairs (pump and signal) will be phase-matched, a calculation is done using the data of Rugar and Foster, who characterize the dispersion in terms of the parameter α, where:

$$\omega(k) = ck\,(\,1 + \alpha k^2\,) \qquad (4.1)$$

with ω the circular frequency ($2\pi f$) and k the wavevector ($2\pi/\lambda$). As a function of the pressure P (in atmospheres) their data form a straight line ($r^2 = .99$):

$$\alpha(P) = (1.531 - 0.1039\ P(\text{in bar})\,) * 10^{-20}\text{m}^2 \qquad (4.2)$$

Referring again to Fig. 4.1, the 30° bevel will cause sound to refract to an angle (with the normal) of roughly 0.6° (actually the angle will also change slightly with pressure due to the change in sound speed c). Using the dispersion relations in Eqs. (4.1) and (4.2), then, for example, at 2.6 bar, a 4.5 GHz pump will be correctly phase-matched to a 2.6 GHz signal.

2. First Experimental Design

The first experimental attempt at constructing an all-acoustic parametric amplifier in superfluid helium used a multifaceted-crystal design (see Fig. 4.2). The transducers are positioned to overlap as the beams exit the sapphire piece at the bottom, near the bevel intersection. A small part of the signal from the transducer on the top bevel (tilted) surface reflects from the bottom bevel (carefully polished to be parallel to the upper bevel). It was intended that this return could be used to tune the bevel transducer, so as to optimize its power output near the pump frequency, in the hope of maximizing the gain of the amplifier. The experiment was attempted several times, but the reflected signal from the bottom flat (the helium signal) was never seen. An attempt was made to place another transducer at the bottom of the cell, to operate the experiment in transmission. The shape of the top crystal made it extremely

TRANSDUCER SIDE

PUMP
(BEVEL)

SIGNAL
(MAIN)

Antireflection coating
(amorphous carbon)
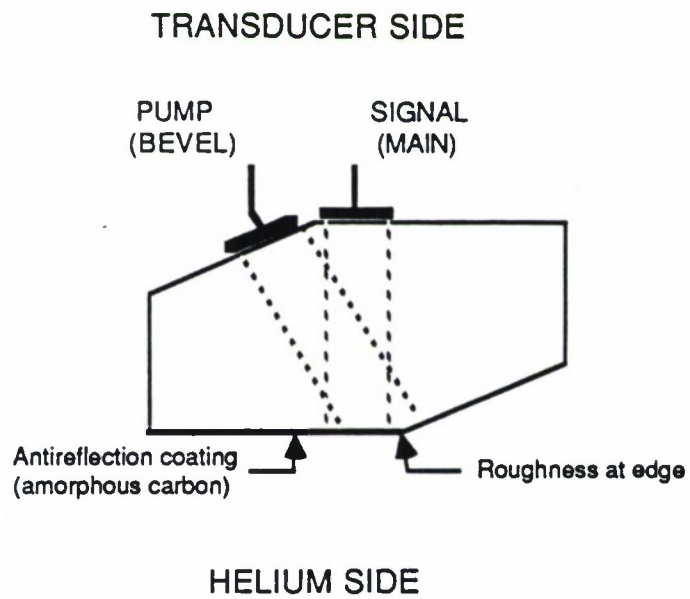
Roughness at edge

HELIUM SIDE

FIGURE 4.2 Parametric Amplifier crystal geometry for first
experimental try, using doubly-beveled crystal. The flat
bottom (reflecting) crystal is not shown.

difficult to attempt to align laterally the transducers on the two crystals, so the system could not be tested in water (at room temperature). Also, despite obtaining return sapphire echoes from the bevel, one could never be sure just how well the beams overlapped, if at all.

In retrospect, the main reason for failure was the geometry of the top crystal. Crystals used in superfluid helium acoustics usually use a matching (antireflection coating) layer, typically of amorphous carbon with a thickness of a quarter-wavelength (for the center frequency desired). The bevel surface, however, meant that the sapphire surface was not perfectly flat and parallel all the way to the edge, since polishing techniques, despite great care, cannot prevent cracking and splintering close to the edge. The carbon matching layer thus also went down poorly, with imperfections near the edge (which is precisely where the experimental beam was centered). Although the crystal used in the experiments looked visually smooth near the beam exit point, problems in adhesion on some of the other crystals made in the same run, in some cases even peeling off the carbon layer, suggest that even the experimental crystal may have had enough unevenness in the surface and/or matching layer thickness (especially on the 1000 Å scale of the helium wavelength) so as to give a poor transfer into the helium, allowing at best a wave of poorly-defined phase-front to be transmitted.

3. New Design

The new design adopted when the decision was made to repeat the parametric amplifier experiment solves many of the worst problems of the first design. The new geometry has the bevel surface on the transducer side *only*, with the carbon side (helium side) flat. By giving up a chance to tune the bevel transducer much has been gained. The absence of a bottom edge means that the sapphire can be polished more easily and more flat, and the amorphous carbon matching layer can be deposited more evenly, for good beam throughput.

The new design also required a change in the photolithography technique used to define the transducers for "liftoff" on the crystal surface (in "liftoff" the gold is deposited everywhere atop the photoresist, and upon use of a solvent for the photoresist, peels away everywhere except where the

photoresist has been previously removed). Under the old design the main (flat) transducer was defined in a projection microscope, its distance to the edge measured (using a reticuled eyepiece in the microscope), and the position of the bevel transducer calculated by a program taking into account the walk-off in the (anisotropic) sapphire. This new position was then obtained by looking through the microscope and translating the sample, using the reticule and small specks of dust as milestones. The distance traveled was usually two to four fields-of-view of the microscope, which presented a dangerously easy source of error. In the new design, without the bottom bevel to test the reflection, the placement of the bevel transducer had to be correct the first time--and especially since the first run had had no results it was determined that the new run should eliminate as many sources of error as possible. (Later it was also learned that the position of the beveled transducer "footprint" could be determined directly using small latex spheres, discussed later).

The new photolithography technique uses a single exposure through an electron-beam-defined contact mask (see Fig. 4.3). The calculation of relative placement was thus done one time (though rechecked many times, of course, before programming the e-beam machine to write the mask) and the mask for both transducers located relative to the bevel edge using alignment "windows" defined in the mask. Naturally, since the crystal has a bevel, the mask will be a contact mask only on the flat surface and a projection mask on the tilted surface. For that reason both of the holes were made below size (and in fact the "bevel" hole was made elliptical so its projection would be round). Thus after alignment and exposure in the Kasper mask aligner the photoresist was partially developed to reveal a small mark. The crystal is then put under the projection microscope and a sharp round hole of the correct size is exposed on top of the mark. The crystal is then placed in a special tilted holder and a round mark exposed on the bevel also. In that way the holes in the photoresist are correctly sized and sharp, with steep walls to make the lift-off process work better.
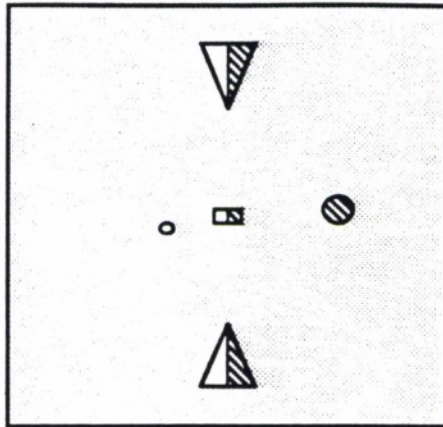
(a) Top View
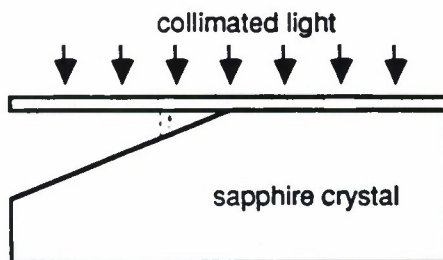
(b) Side View

FIGURE 4.3 Photolithography of transducers for Parametric Amplifier experiment. (a) Top view of mask showing alignment windows and exposure circles, adjusted to counteract acoustic beam walkoff in crystal. (b) Side view showing initial exposure.

4. Experiment One

The first experiment produced some startling results. Gain at the correct "phase-matching" was very small, and a larger gain was seen in a collinear interaction at a different frequency.

At the start of the experiment, gain was noticed when the signal and idler frequencies were close to each other, surprising since for the planned noncollinear interaction such frequency pairs are very phase-mismatched. Typical results are shown in Fig. 4.4, which monitors the output power at the 3360 MHz signal as the 3800 MHz pump power is increased. Notice, from (b), that the gain is still present on the beta pulse; in fact, it is larger! Thus the dominant interaction here must be between waves traveling in the same direction. Figure 4.5 shows the maximum gain as the pump frequency is varied, thus giving the bandwidth of the process.

The behavior of the pump signal was also monitored as the signal power was varied. Figure 4.6 (a) shows the power-out/power-in curve for the pump alone (no signal power). The graph shows the usual linear climb, then sudden saturation and drop as the result of runaway amplification of the noise. The second small additional increase some 30 dB after the saturation point possibly represents the detection of an outer lobe of the bevel signal (since the bevel transducer is significantly less efficient). Also shown are two points marking the "small" and "large" powers chosen for part (b). Figure 4.6 (b) shows the behavior of a fixed input pump power as the signal power is increased. In both cases the pump is depleted, but note that the small pump actually experiences gain! For power to flow to the higher frequency, it must be the case that the driving "effective" pump is the harmonic of the stronger input beam.

After some search, gain was finally found where it was supposed to be. Figure 4.7 shows the maximum gain on the alpha signal (there was no gain on the beta signal) for the calculated noncollinear phasematched frequencies of 2.545 GHz for the signal and various pump frequencies, at an intermediate pathlength, d=0.72 mm. More details on all of this can be found in the thesis by Wright.[45]

(a) Alpha Pulse Gain

Input Power of 3800 MHz Pump (dB)

(b) Beta Pulse Gain
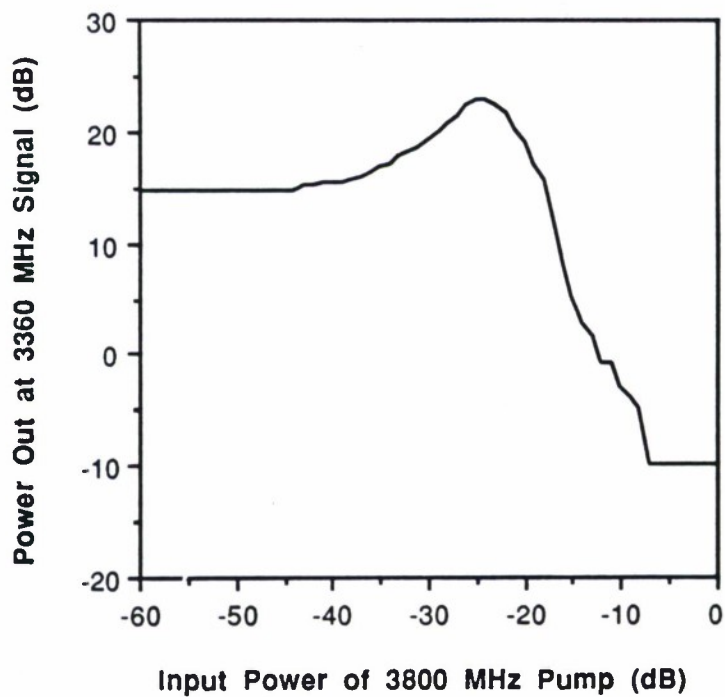

Input Power of 3800 MHz Pump (dB)
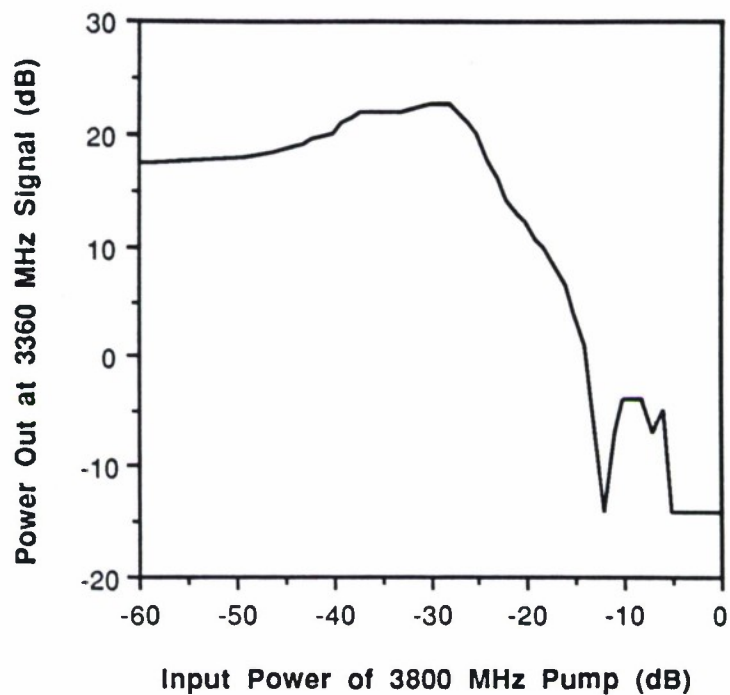
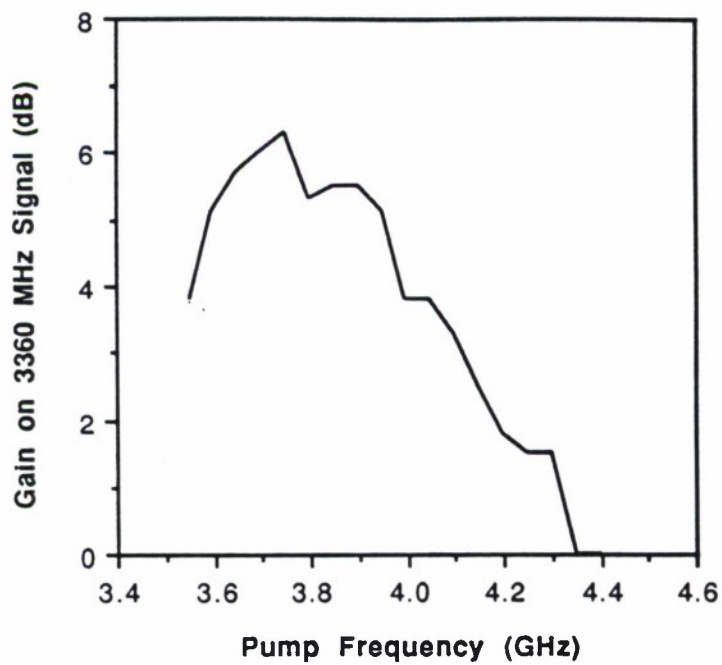FIGURE 4.4 Signal Power Received as Pump Power is varied for (a) alpha and (b) beta pulses. Both experience gain.

FIGURE 4.5 Maximum Gain of alpha pulse of signal as a function of pump frequency, thus giving Gain Bandwidth. d=0.70 mm.

(a) 3800 MHz Pump Only
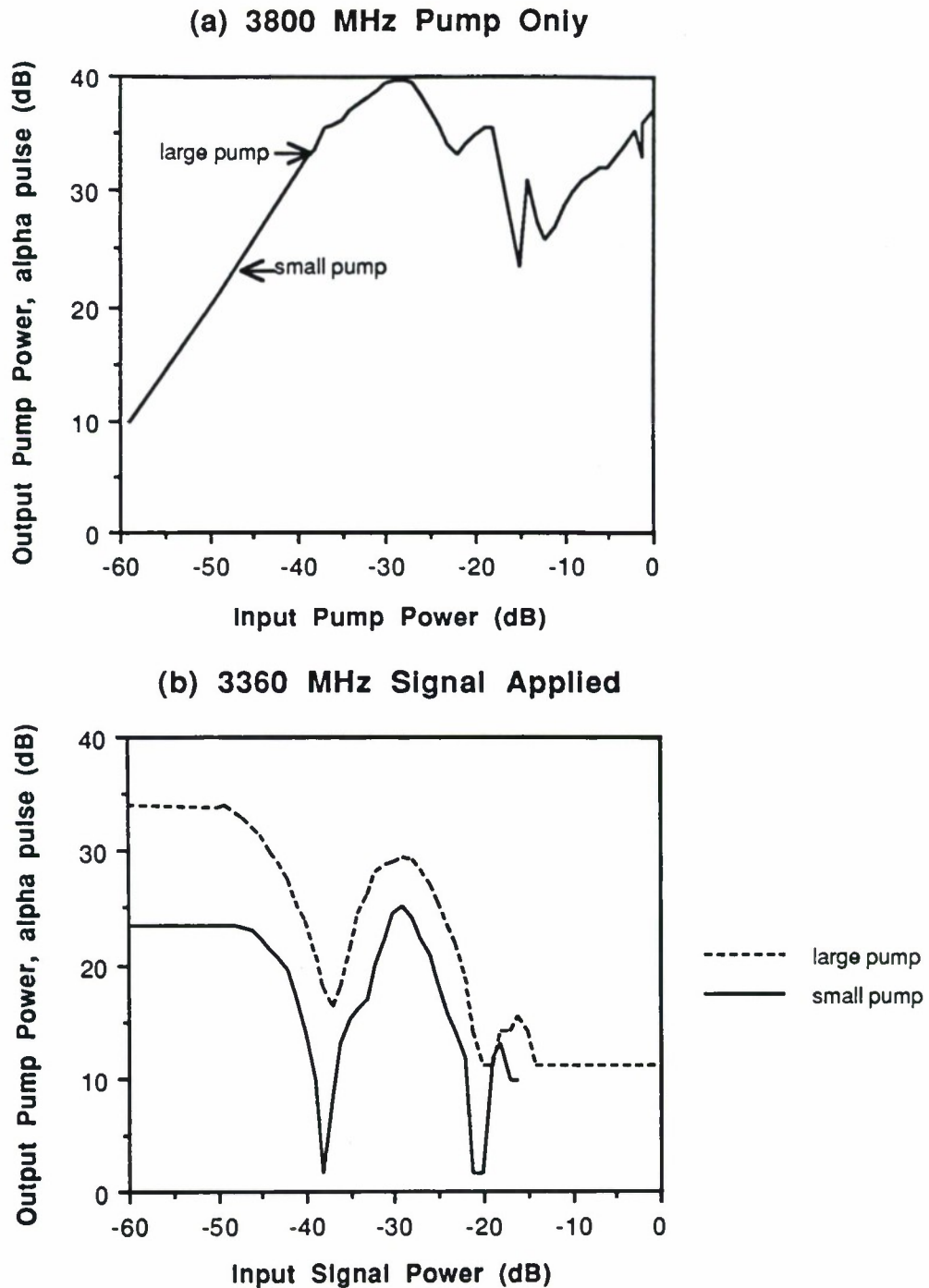

(b) 3360 MHz Signal Applied

FIGURE 4.6 Behavior of Pump in Collinear Gain Process (alpha pulse): (a) Power Out vs. Power In for Pump alone (no signal power applied). (b) Pump Out as Signal Power increased for two different input pump powers. Note gain on small pump.
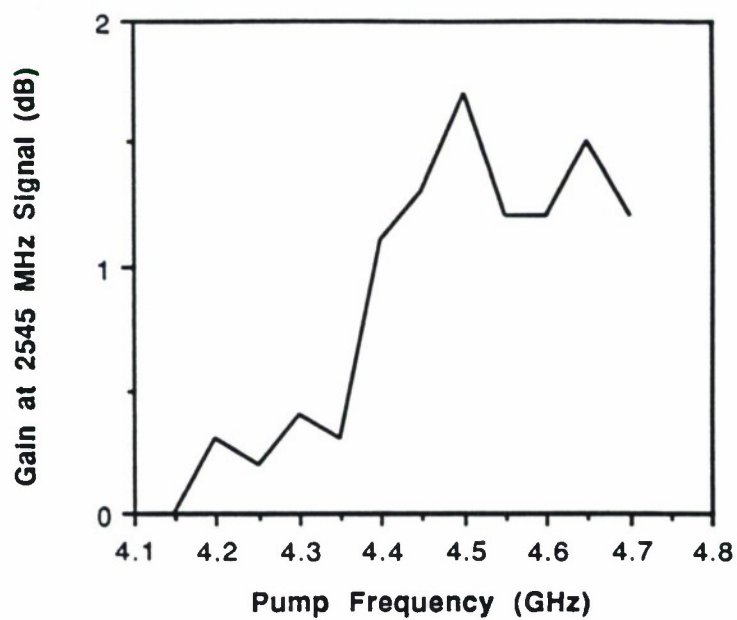
FIGURE 4.7 Noncollinear gain bandwidth, d=0.72 mm. Gain is on alpha pulse only (no gain on beta pulse).

V. Acoustic Microscopy at 15.3 GHz

At the conclusion of this program we furnished a multilayer transducer to M.S. Muha at the Aerospace Corporation for their use in a Scanning Acoustic Microscope at 15.3 GHz. The following is abstracted from their publication.[46]

"The highest-resolution acoustic microscopes have been diffraction limited, so to achieve higher resolution an acoustic microscope must utilize a shorter wavelength. The shortest wavelength that can be used depends on the choice of the fluid that couples the acoustic energy from the lens to the object. An acoustic microscope using water as the coupling medium achieved a resolution of 2000 Å at a frequency of 5 GHz. Further improvement in resolution for a water acoustic microscope is hampered by a low signal-to-noise ratio, which is caused by an increasing acoustic attenuation in water as the frequency is increased. Better resolution can be achieved by using as the coupling fluid unpressurized superfluid ^{4}He at temperatures below 0.2 K, because of its low acoustic attenuation and low sound velocity. An acoustic microscope operating in unpressurized superfluid ^{4}He at a temperature of 0.1 K achieved a resolution of 200 Å at a frequency of 8 GHz. Further improvement in resolution in such a cryogenic acoustic microscope is limited by a low signal-to-noise ratio, which results when acoustic nonlinearities in the superfluid helium cause the received signal to saturate and then decrease as the input power is increased. The maximum received signal (at saturation) decreases as the frequency of operation is increased. The acoustic nonlinearity believed to be responsible for this limitation in received signal is the three-phonon spontaneous decay of the input signal at a frequency of ω_p and a wavenumber of k_p into decay products at frequencies ω_1, ω_2 and wavenumbers k_1, k_2, where energy and momentum conservation must be satisfied, i.e.,

$$\omega_1 + \omega_2 = \omega_p \; ; \; k_1 + k_2 = k_p \qquad (1)$$

This spontaneous decay process is self-enhanced in a parametric process at high sound intensities such as are found at the focus of an acoustic lens.

The acoustic microscope reported here eliminates parametrically self-enhanced spontaneous decay by employing ^{4}He pressurized to greater than 20 bar. For Eq. (1) to be satisfied, it is necessary for the sound-dispersion curve to be anomalous; that is, the speed of sound must increase with increasing frequency. Below 20 bar, ^{4}He has an anomalous sound-dispersion curve. Pressurizing the superfluid helium to above 20 bar causes the dispersion curve to be normal (i.e., the speed of sound decreases with increasing frequency) at all frequencies, so that three-phonon spontaneous decay [Eq. (1)] is forbidden. In fact, the spontaneous decay of a single phonon into any number of phonons is prohibited. The received signal is then no longer limited by spontaneous decay. A different saturation mechanism still occurs in helium pressurized above 20 bar, but onlyu at a much higher power level. For example, D. R. Wright *et al.*, measured an increase of 15 dB in maximum received signal of when the pressure was increased from 8 to 22 bar. They attributed the saturation in received signal in helium pressurized above 20 bar to a four-phonon process, where two signal phonons combine to produce two new phonons at different frequencies.

Pressurizing the helium above 20 bar also eliminates another source of acoustic attenuation: the scattering of the signal phonons by thermal phonons in a three-phonon process. This process is forbidden by conservation of energy and momentum in a fluid having normal dispersion. With this thermal-phonon scattering eliminated, the only significant source of attenuation in the fluid below 0.9 K is the four-phonon scattering referred to above. At temperatures above 0.9 K the attenuation becomes large, possibly because of roton scattering. Hence a microscope using superfluid ^{4}He pressurized above 20 bar can be operated up to approximately 0.9 K, while an unpressurized microscope must be operated below 0.2 K to avoid thermal-phonon scattering. The acoustic microscope described here is cooled by a sorption-pumped ^{3}He cryostat to 0.4 K, while

the unpressurized ^{4}He microscope reported earlier required a dilution refrigerator for cooling below 0.2 K.

The heart of the acoustic microscope is a c-axis-oriented sapphire rod having an acoustic transducer on one end and an acoustic lens on the other. The acoustic lens element is a polished spherical depression ground on one end of the sapphire rod. An 800-Å-thick layer of amorphous carbon evaporated on the lens surface serves as a matching layer to reduce the large acoustic impedance mismatch between sapphire and liquid helium. A 400 Å thick layer of molybdenum is evaporated before the carbon is deposited to increase the adhesion between the carbon film and the sapphire substrate and to improve the impedance matching. The acoustic transducer is a multilayer ZnO piezoelectric thin film. Each layer is 1700 Å thick, and the crystal orientation of alternate layers is varied to attain periodic coefficients of piezoelectric coupling. This type of multilayer transducer presents a higher impedance to the incoming microwave pulses, resulting in a better match and a higher conversion efficiency than would be possible at 15.3 GHz with the single-layer transducers previously used. The measured one-way conversion loss of the multilayer transducer is 15 dB."

This instrument is now operational. It is used for recording images of IC devices with a resolution of 150 Å.

References

1. T.M. Reeder and D.K. Winslow, IEEE Trans. MTT, **MTT-17**, 927 (1969).

2. B.A. Auld, *Acoustic Fields and Waves in Solids*, Vol 1 (Wiley-Interscience, New York, 1973).

3. B. Hadimioglu, "High Resolution Acoustic Microscopy," Ph.D. Dissertation, Stanford University (1985).

4. J. Foster, "Superfluid Helium Acoustic Microscopy," Ph.D. Dissertation, Stanford University (1984).

5. H.J. Shaw, "Selected Studies in Microwave Acoustics," Microwave Laboratory Report No. 1382, Stanford University (1965).

6. J. de Klerk, P.G. Klemens and E.F. Kelly, Appl. Phys. Lett. **7**, 264 (1965).

7. K.H. Yang, P.L. Richards, and Y.R. Shen, J. Appl. Phys. **44**, 1417 (1973).

8. H.K. Wong, G.K. Wong and J.B. Ketterson, J. Appl. Phys. **53**, 6834 (1982).

9. P. Roden and G.H. Dohler, Solid State Commun. **45,** 23 (1983).

10. J.J. Quinn, U. Strom and L.L. Chang, Solid State Commun. **45**, 111 (1983).

11. B. Hadimioglu, B.T. Khuri-Yakub, L.G. Goddard and C.F. Quate, Proc. 1986 IEEE Ultrasonics Symp., 361 (1986).

12. N.F. Foster, G.A. Conquin, G.A. Rozgonyi and F.A. Vannatta, IEEE Trans. Sonics and Ultra., **SU-15**, 28 (1968).

13. J.S. Wang and K.M. Larkin, Proc. IEEE 1982 Ultrasonics Symp., 480 (1982).

14. L.M. Brekhovskikh, *Waves in Layered Media*, translated by D. Lieberman (Academic Press, New York, 1960).

15. R.C. Bray, "Acoustic and Photoacoustic Microscopy", Ph.D. Dissertation, Stanford University (1979).

16. M.V. Schneider, B. Glance, and W.F. Bodtmann, Bell System Tech. J. **48**, 1703 (1969).

17. B. Hadimioglu, L.J. LaComb, Jr., L.C. Goddard, B.T. Khuri-Yakub and C.F. Quate, Proc. 1987 IEEE Ultrasonics Symp., 717 (1987).

18. D. Howell, L.C. Goddard and B.T. Khuri-Yakub, Proc. 1987 IEEE Ultrasonics Symp., 381 (1987).

19. L.J. LaComb, Jr., B.T. Khuri-Yakub, C.F. Quate and B. Hadimioglu, Proc. 1988 IEEE Ultrasonics Symp., 327 (1988)

20. E.K. Sittig, IEEE Trans. Sonics and Ultrasonics, SU-14, 167 (1967).

21. J. Ilukor and E.H. Jacobsen, in *Physical Acoustics*, edited by W.P. Mason (Academic Press, New York, 1968), Vol V.

22. R.C. Dynes and V. Narayanamurti, Phys. Rev. B, 12, 1720 (1975).

23. D. Rugar, J. Appl. Phys. 56, 1338 (1984).

24. J.S. Foster, "Superfluid Helium Acoustic Microscopy," Ph.D. Dissertation, Stanford University (1984).

25. M. Cabot and S. Putterman, Phys. Lett. 83A, 91 (1981).

26. M. Cabot and S. Putterman, Proceedings of the 16th International Conference on Low Temperature Physics (LT16: Los Angeles, 1981), in *Physica* 107B, 107 (1981).

27. J.S. Foster and S. Putterman, Phys. Rev. Lett. 54, 1810 (1985).

28. S.A. Akhmanov, V.V. Fadeev, R.V. Khokhlov, and O.N. Chunaev, Sov. Phys. JETP Lett. 6, 85 (1967).

29. D. Magde and H. Mahr, Phys. Rev. Lett. 18, 905 (1967).

30. S.E. Harris, M.K. Oshman and R.L. Byer, Phys. Rev. Lett. 18, 732 (1967).

31. R.L. Byer, "Parametric Fluorescence and Optical Parametric Oscillation", Ph.D. Dissertation, Stanford University (1968).

32. R.L. Byer and S.E. Harris, Phys. Rev. 168, 1064 (1968)

33. R.C. Dynes and V. Narayanamurti, Phys. Rev. B, 12, 1720 (1975).

34. D. Rugar and J.S. Foster, Phys. Rev. B, 30, 2595 (1984).

35. D.R. Wright, B. Hadimioglu, L.J. LaComb, Jr., C.F. Quate and J.S. Foster, Jap. J. Appl. Phys. **26**, 9 (1987).

36. H.J. Maris, Rev. Mod. Phys. **49**, 341 (1977).

37. R. Esche, Akustische Beihefte, supplement to Acustica, **2AB**, 208 (1952).

38. E.A. Neppiras, J. Acoust. Soc. Am. **46**, 587 (1969).

39. R.D. Finch, R. Kagiwada, M. Barmatz and I. Rudnick, Phys. Rev. **134**, A1425 (1964).

40. R.F. Carey, J.A. Rooney and C.W. Smith, J. Acoust. Soc. Am. **66**, 1801 (1979).

41. F.P. Milliken, K.W. Schwartz and C.W. Smith, Phys. Rev. Lett. **48**, 1204 (1982).

42. T.E. Huber and H.J. Maris, Phys. Rev. Lett. **47**, 1907 (1981).

43. D.L. Weinberg, Appl. Phys. Lett. **14**, 32 (1969).

44. J.G. Meadors, W.T. Kavage and E.K. Damon, Appl. Phys. Lett. **14**, 360 (1969).

45. D.R. Wright, "Nonlinear Acoustic Interactions in Superfluid Helium," Ph.D. Dissertation, Stanford University (1989).

46. M.S. Muha, A.A. Moulthrop, G.C. Kozlowski and B. Hadimioglu, Appl. Phys. Lett. **56**, 1019 (1990).

Technical Reports

Status Report	June 1 - September 30, 1987
Status Report	April 1 - September 30, 1988
Annual Report	June 1, 1987 - September 30, 1988

Publications

"Piezodriven Scanner for Cryogenic Applications"
Lloyd J. LaComb, Jr. & C. F. Quate
Rev. Sci. Instrum., **59**, 1906-10 (1988)
(Partially supported by the National Science Foundation)

"Interface Structure of Multilayer ZnO Acoustic Transducers"
L. J. LaComb, Jr., B.T. Khuri-Yakub, C. F. Quate & B. Hadimioglu
Proc. IEEE 1988 Ultrasonics Symposium, Vol. 2, 327-332 (1988)

"Dependence of Orientation and Electrical Properties in Sputtered ZnO Upon
Deposition Conditions and Substrate"
M. D. Howell, S. Akamine, L. J. LaComb, Jr., B. Hadimioglu, T. R. Albrecht,
B. T. Khuri-Yakub, L. C. Goddard & T. E. Carver
Proc. IEEE 1988 Ultrasonics Symposium, Vol. 2, 677-680 (1988)
(Partially supported by the Defense Advanced Research Projects Agency)

Unpublished:

"Foundations of Millimeter-Wave Acoustic Microscopy"
L. J. LaComb, Jr.
Ph.D. Dissertation, Stanford University, June 1989
(Partially supported by the Defense Advanced Research Projects Agency)

"Nonlinear Acoustic Interactions in Superfluid Helium"
D. R. Wright
Ph.D. Dissertation, Stanford University, June 1989.